Thermal fluctuations and stability of solid-supported lipid membranes

2005 J. Phys.: Condens. Matter 17 R287

(http://iopscience.iop.org/0953-8984/17/6/R02)

INSTITUTE OF PHYSICS PUBLISHING JOURNAL OF PHYSICS: CONDENSED MATTER

J. Phys.: Condens. Matter **17** (2005) R287–R314 doi:10.1088/0953-8984/17/6/R02

TOPICAL REVIEW

Thermal fluctuations and stability of solid-supported lipid membranes

Tim Salditt

Institut für Röntgenphysik, Georg-August-Universität Göttingen, Geiststraße 11, 37073 Göttingen, Germany

E-mail: tsaldit@gwdg.de

Received 1 June 2004, in final form 4 January 2005
Published 28 January 2005
Online at stacks.iop.org/JPhysCM/17/R287

Abstract

In this review article we discuss recent work on the thermal stability, thermal fluctuations and interaction forces in lipid membrane stacks. The lipid bilayers are deposited on solid surfaces for investigation by interface sensitive x-ray and neutron scattering on length scales ranging from the molecular to the mesoscopic scale. We discuss how the structure, composition, fluctuations, and interactions in lipid and biomimetic membranes can be studied in the fluid L_α phase. Results on the interaction potentials, height–height correlation functions, elasticity parameters, fluid lipid chain ordering, and collective lipid chain motions are discussed.

(Some figures in this article are in colour only in the electronic version)

Contents

0953-8984/05/060287+28$30.00

1. Introduction

Phospholipid membranes are regarded as simple model systems for more complex biological counterparts [1]. At the same time, fluid membranes have received much attention as a paradigmatic example of self-assembled complex fluids which exhibit unique elasticity, interaction, and transport properties. Thermal fluctuations of lipid membranes on molecular to mesoscopic scales reflect physical properties such as thermodynamic stability, self-assembly, elasticity, interaction potentials, and phase transitions of the lipid bilayers [1]. Reciprocally, fluctuations may strongly influence these phenomena. This interplay is of interest in simple model lipids, as well as in more complex multi-compartment bilayer systems, and certainly also in biological membranes containing functional membrane proteins [2, 3]. From high-resolution x-ray and neutron scattering of lipid bilayer phases followed by peak lineshape analysis, the thermal fluctuations have been probed [4–7]. To this end, multilamellar phases of stacked lipid bilayers exhibit smectic liquid-crystalline (LC) symmetry, and much of the physics involved can be understood from a general consideration of the smectic LC state; see e.g. [8] for an excellent review. Multilamellar samples also allow for a tremendous increase in scattering volume over single-bilayer or more dispersed phases. Finally, inter-bilayer interaction potentials [9, 10] can be determined from such studies, e.g. by controlling the osmotic pressures and thus the total molecular forces acting between membranes [9].

While most structural studies have been carried out on isotropic suspensions in aqueous solution, the advantages of highly aligned films are increasingly used, first to deduce the detailed structure of lipid bilayers in gel phases [11–13], more recently also in the fluid phase [14, 15]. By specular x-ray and neutron reflectivity single bilayers [16–18] or monolayers [19] are also detectable. Short wavelength radiation (neutrons or x-rays) allows for the measurement of the scattering length density profile along the membrane normal on an absolute scale. Non-specular reflectivity, grazing incidence diffraction, and reciprocal space mappings give access to the structure in the plane of the bilayer (lateral structure). For an introduction to interface sensitive scattering see the recent monographs [20, 21]. As often in scattering, neutron and x-rays complement each other. While x-ray beams are typically more brilliant, neutrons allow for different contrast as well as variation of contrast. Most importantly, inelastic neutron scattering (INS) provides a unique method to study the collective dynamics (dispersion relations) of the lipid molecules.

Owing to their symmetry, lamellar phases lend themselves to deposition on and coupling to a solid surface. Molecular structure, interaction forces, elasticity parameters and fluctuation properties can then be studied with powerful surface analytical techniques. Functional molecules such as membrane-active proteins can be incorporated, offering a great potential for material science and biotechnology. Finally, chemical reactions like binding of molecules, release of bound molecules and changes in the film properties resulting from changes in the environments (chemical potentials, electrical and magnetic fields, optical excitation) can be studied in thin films. Low mosaicities, i.e. sharp distributions of bilayer normal vectors with respect to the film boundaries, on the order of 0.01° enable a precise distinction between the scattering vector component normal q_z and parallel q_r to the bilayer; see figure 1.

In this paper, we review recent work on pure lipid phases in the physiologically relevant liquid L_α phase at conditions of low osmotic pressure (where water availability is high). However, the methods used can be applied to probe the structure and interaction of lipid bilayers with membrane-active molecules and polypeptides (such as stereols, peptides, proteins). Organization of the paper: following this introduction, section 2 discusses experimental aspects of sample preparation, sample environments and technical aspects of scattering experiments on aligned lipid membranes 2. Section 3 is a brief summary of the simplest linear model to

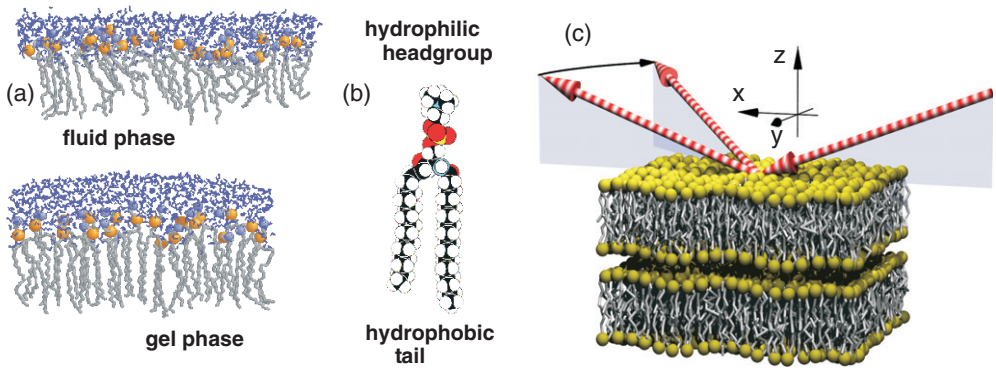

Figure 1. (a) One leaflet of a phospholipid bilayer in the more ordered gel and fluid phase (at higher temperatures) (from [22]). (b) Lipid molecule with hydrophilic headgroup and hydrophobic tails. (c) Schematic diagram of two planar lipid bilayers with incident, reflected and scattered beams.

describe the thermal fluctuations of membranes with smectic liquid-crystalline (LC) symmetry. Section 5 covers the structural analysis by specular x-ray and neutron reflectivity (SXNS, SXR), while section 6 covers non-specular (diffuse) x-ray and neutron reflectivity (NSXR, NSNR) from lipid membranes. Section 7 is dedicated to the issues of thermal stability and unbinding. Finally, section 8 briefly addresses the short range order of lipid molecules in the fluid state of the bilayer, as studied both by elastic scattering and inelastic neutron scattering (INS).

2. Experimental aspects

2.1. Sample preparation

Films of lipid membranes can be prepared using the classical procedure of spreading lipids (and peptides) from solution [23], as free standing films [24], or by more recent schemes which allow for a precise control of the total number of bilayers N by spin-coating the solutions [25]. Novel methods to prepare single or double bilayers have also proven very useful [17]. Thus, bilayer stacks with one, few and up to several thousand layers can be obtained with a high orientation and for many different neutral or charged phospholipids and lipid mixtures [26, 15]. Membranes can be deposited on a large variety of substrate such as classical silicon wafers, glass microscopy slides, or mica sheets. As an example let us consider solutions of a few tens of milligrams of 1,2-dimyristoyl-sn-glycero-3-phosphatidylcholine (DMPC) dissolved in 1 ml of isopropanol and spread on clean silicon wafers. After removing the organic solvent by putting the samples in a desiccator for few hours and after rehydration in humid air, a highly aligned multilamellar film with a mosaic spreading typically better than 0.01° and a total thickness in the range of 10 μm is formed see the schematic in figure 2(a).

2.2. Sample environment

Different sample environment chambers for control of temperature, humidity, and other control parameters (osmotic pressure, electrical fields) have been reported, with considerable recent progress. For example, it was long taken for granted that uncharged membranes could not be swollen to their equilibrium periodicity d_0 in water vapour, even if the water vapour was (nominally) at 100% relative humidity. This phenomenon had been termed the vapour pressure

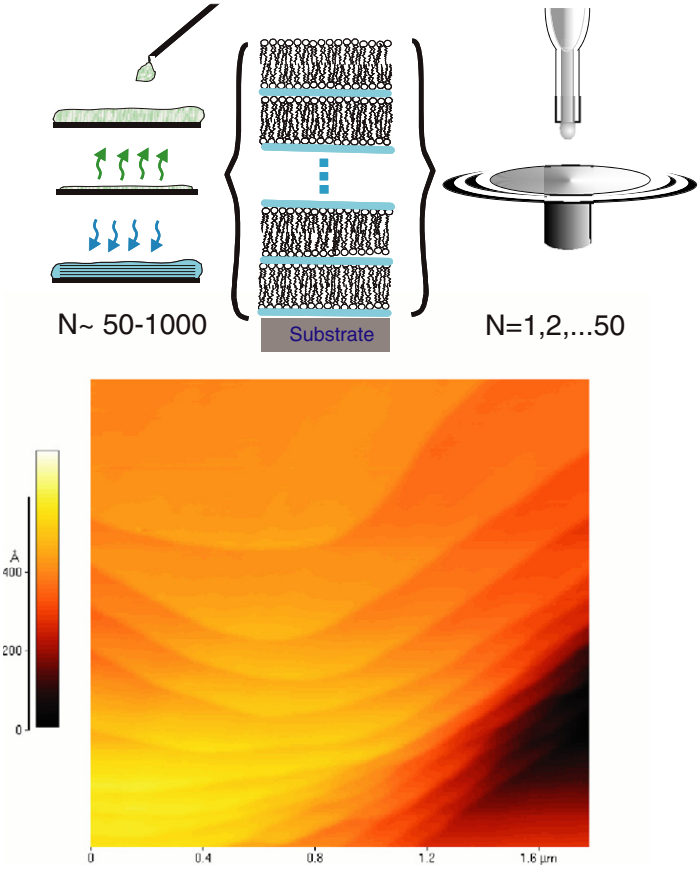

Figure 2. Sample environment for solid supported and oriented membranes. Schematic diagram of sample preparation by (a) spreading from organic solvent and subsequent evaporation (thick multi-lamellar stacks) and (b) spin-coating a droplet of solution on the substrate (thin oligo-lamellar stacks). (c) AFM micrograph at the edge of a DMPC oligo-bilayer patch (Park Scientific, tapping mode, lateral range of about 1.8 μm, from [27]). The vertical steps correspond to integer numbers of bilayers.

paradox, but was subsequently demonstrated to result from small temperature gradients in the sample chamber [28], making initial explanations which were based on the suppression of thermal fluctuations obsolete. At the same time, it could be shown that full hydration can be reached in humidity chambers of appropriate design [28, 17]. It was also demonstrated that solid-supported lipid films can be studied while immersed in excess water [29]. This is of interest for two reasons: firstly, excess water warrants the physiologically relevant condition of full hydration. Secondly, membrane active molecules can be adsorbed directly from the solution. The interaction between the multilamellar stack and the macromolecules can be studied *in situ*, including the dynamics of adsorption and desorption. However, films in excess water are unstable in the absence of osmotic agents (stressors).

Imposing the osmotic pressure (Π, N m^{-2}) to multilamellar phases is a unique method for studying bilayer interactions [30] since pressure is equivalent to the force per unit surface between parallel stacked membranes. Thus, the pressure–distance relationship of bio-molecular assemblies can be addressed and bilayer undulations or compressibility fluctuations can be studied as a function of pressure. High pressures are imposed by the vapour phase of

saturated salt solutions [30, 31]. Low pressures are imposed immersing the sample in a polymer stressor solution of a few weight per cent. This well known technique for bulk suspensions was recently extended to oriented lamellar phases [32]. For charged bilayers, high mass polyelectrolytes of the same sign and counter-ions have been used as osmotic stressors [33]. The imposed pressure corresponds to water layer thicknesses in the range of a few water molecules (5 Å at $\Pi = 10^{6.63}$ Pa) up to more than 15 times the bilayer thickness (320 Å at $\Pi = 10^{3.82}$ Pa). For highly charged bilayers, the interactions are expected to be dominated by electrostatic repulsion in the fully hydrated state. Other inter-bilayer interactions [10] which come into play are dispersion or van der Waals forces, hydration forces, molecular protrusion forces, or entropically driven repulsive forces [34].

For the data shown here, some of the lipid bilayer films have been kept at partial hydration with the bilayers facing water vapour. In this case, a chamber with two concentric high purity aluminium cylinders is used, see figure 3. The inner cylinder is heated or cooled by a flow of oil, connected to a temperature controlled reservoir (Julabo, Germany) with PID control. The space between the two cylinders can be evacuated to minimize heat conduction. The temperature as measured by a $Pt100$ sensor, indicated a thermal stability of better than 0.05 K over several hours [35]. At the bottom of the inner cylinder a water reservoir was filled with salt free Millipore water, such that the sample is effectively facing a vapour phase of nominally 100% relative humidity. Despite the nominally full hydration condition, in this chamber the DMPC bilayers typically swell only up to a repeat distance of $d \simeq 50$–55 Å in the fluid L_α-phase, i.e. were only partially hydrated. We have also used a chamber which allows for full hydration without immersing the sample in water, as evidenced by the well known equilibrium d-spacing for DMPC. This is achieved by a design where the temperature of the water bath can be separately controlled and a small difference in temperature of the bath with respect to the sample leads to full hydration [17]. Alternatively a chamber operating at full hydration can be used where the bilayers are immersed in water, and the beam impinges through a thick Si block (neutrons) or through kapton windows (x-rays) [29]. Conditions of full hydration are important, since the diffuse (nonspecular) scattering from partially hydrated films seems to be easily dominated by static defect scattering, e.g. diffuse scattering from the smectic strain around liquid crystalline defects in the film [14]. At full hydration, thermal fluctuations are stronger and therefore have a larger effect on the diffuse scattering. Furthermore, it is desirable to probe the elasticity and fluctuation properties in the physiologically relevant state of full hydration.

2.3. Neutron and x-ray reflectivity

Measurements have been carried out over a wide range of vertical momentum transfer q_z and parallel momentum transfer $q_r = \sqrt{q_x^2 + q_y^2} = 0$. Measurements at fixed vertical momentum transfer (e.g. for constant $q_z = 2\pi/d_z$) and at varied q_r have been used to probe lateral length scales between a few ångström up to several microns. Thereby, the diffuse scattering, due to fluctuations and to the short range order due to the lateral packing of the lipid molecules can be measured. Different combinations of line scans as well as mesh scans, i.e. mappings of reciprocal space (RSM) in q_z and q_x have been used. In addition, data have been collected by 2D detectors (CCD cameras, image plates). Pure specular x-ray reflectivity (SXR) has been measured at in-house sealed tube reflectometers, while non-specular diffuse reflectivity (NSXR) and RSM necessitate synchroton radiation. Several beamtimes at the D4 bending magnet of HASYLAB/DESY in Hamburg, and at the ID1 undulator station of ESRF in Grenoble, have provided the data shown here. Neutron reflectivity (SNR) experiments have been performed on the Adam [36, 26] and D17 reflectometers [37, 38] at ILL. Inelastic

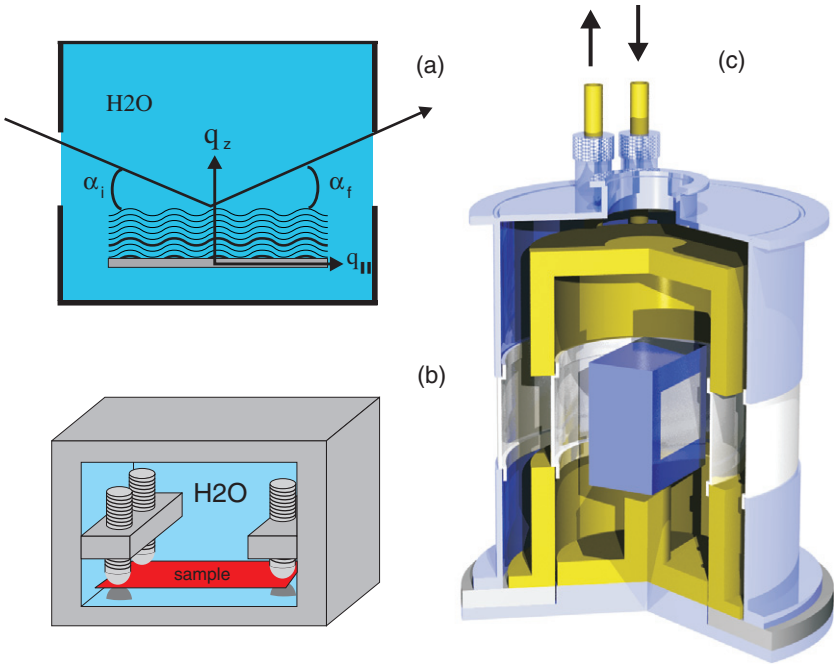

Figure 3. Sample environment for solid supported and oriented membranes. (a) Schematic diagram and (b) sketch of the experimental cell used for measurements in excess water which allows for *in situ* experiments (osmotic stress, absorption, desorption, ion exchange). (c) The cell is then placed into a temperature chamber consisting of two concentric cylinders with aluminium (neutrons) or kapton (x-rays) windows. The latter chamber can also be used for studies in water vapour (humidity cell), with direct exposure of the samples to the vapour phase.

measurements (INS) have been carried out at the IN12 spectrometer [39]. The option of contrast variation which is widely used in specular neutron reflectometry [16, 18] allows specific labelling of molecular groups. Nonspecular neutron reflectivity (NSNR) of lipid membranes has been investigated in a series of experiments using monochromatic neutrons of fixed wavelength [26]. Neutron reflectivity in time-of-flight (TOF) mode allows for simultaneous collection of neutrons over a range of wavelengths, significantly reducing accumulation time. In TOF-NSNR neutrons with a broad range of wavelength λ are simultaneously recorded as a function of their respective time of flight, as well as scattering angle on a two-dimensional multiwire detector. Intensity distributions as a function of q_z and q_x can be obtained without moving any motors [37, 38].

3. Linear models of thermal fluctuations and scattering theory

Multilamellar membrane fluctuations can be described by the linearized free energy density of a 3D smectic liquid crystal [34, 4, 5, 40–42]. On large length scales, the finite size effects and the presence of film boundaries (e.g. at the substrate) become apparent and limit the fluctuation amplitudes σ_n of the bilayers [43, 44]. On short length scales the bilayer undulations (bending and compressional modes) can be described by bulk smectic elasticity theory using a discrete displacement field $u_n(r, z)$ for each bilayer [42, 45, 43, 41, 40],

$$H = \int_A \mathrm{d}^2 r \sum_{n=1}^{N-1} \left(\frac{1}{2} \frac{B}{d} (u_{n+1} - u_n)^2 + \frac{1}{2} \kappa \left(\nabla_{xy}^2 u_n \right)^2 \right), \tag{1}$$

where κ denotes the bilayer bending rigidity, A the area in the xy-plane, N the number of bilayers, and u_n the deviation from the mean average position nd of the nth bilayer. B and $K = \kappa/d$ are elastic coefficients, governing the compressional and bending modes of the smectic phase, respectively. Equation (1) is called the discrete smectic Hamiltonian, in contrast to the continuum (Caillé) model, where the sum over n is replaced by an integral. Film boundaries can be accounted for by surface tension terms, which are not included above. From equation (1) or similar Hamiltonians with additional surface terms, the characteristic height–height (displacement) correlation functions $g_{ij}(r) = \langle[u_i(\mathbf{r}') - u_j(\mathbf{r}' + \mathbf{r})]^2\rangle$, can be calculated [41, 40, 44], describing the self and the cross-correlations of the bilayers labelled by i and j [46, 47]. In scattering experiments from bulk suspensions, the full information on the characteristic displacement correlation functions cannot be retrieved due to powder averaging over the different domains in solution. Correspondingly, model assumptions have to be introduced in the data analysis. For large bilayer bending rigidity $\kappa \gg kT$ typical for phospholipid systems, only the combination $\sqrt{KB}$ of the two Caillé moduli B and $K = \kappa/d$ can be inferred from the measured lineshape exponent $\eta = \frac{\pi kT}{2d^2\sqrt{KB}}$. The second fundamental parameter, the smectic penetration length $\Lambda = \sqrt{K/B}$, is usually not accessible, unless the bending rigidity becomes small, $\kappa \simeq kT$ [4, 5]. In contrast, the study of fluctuations in aligned (oriented) lamellar phases on solid substrates does not suffer from similar restrictions [14, 15, 48]. However, the boundary condition of a flat substrate has to be considered explicitly in this case, since the fluctuations are quenched on length scales above $\sqrt{D\Lambda}$, where D is the film thickness. The finite fluctuation amplitude of bilayer n (counted from the substrate) increases in this case as [44]

$$\sigma_n = \eta \left(\frac{d}{\pi}\right)^2 \sum_{n=1}^{N} \frac{1}{2n-1} \sin^2\left(\frac{2n-1}{2}\pi\frac{nd}{L}\right). \tag{2}$$

The correlation functions are characterized by several length scales:

(a) the maximum lateral wavelength of fluctuations $\xi_{\max}$ (finite only in thin films, infinite in bulk systems),
(b) the rms fluctuation amplitude of the nth bilayer σ_n, measured on this lateral length scale $\xi_{\max}$, and
(c) the vertical length scale ξ_z over which the fluctuations of wavelength $\xi_{\max}$ are correlated, defining the conformality; see figure 8.

The conformality or cross-correlations of the bilayer undulations leads to the presence of diffuse Bragg sheets in reciprocal space, as can be directly verified from equation (4). The presence of a sharp specular Bragg peak on top of the diffuse Bragg sheet reflects the fact that the bilayers are flat on a macroscopic length scale. Note that on length scales $r > \xi_{\max}$ the bilayers are essential flat, since the associated smectic damping length $\xi_z \simeq \xi_{\max}^2/\Lambda$ excludes a corresponding relaxation of the profile within the film thickness D. On small length scales $r \ll \xi_{\max}$ the fluctuations are not affected by the film boundaries and should be describable by bulk smectic theory. Note that while $\xi_{\max}$ and ξ_z depend on Λ, σ scales with d^2 and the dimensionless constant $\eta = \frac{\pi kT}{2d^2\sqrt{KB}}$.

The diffuse scattering can be written as a unique transformation of the $g_{ij}(r) = 2\sigma_i\sigma_j - 2c_{ij}(r)$, by [46, 47]

$$S(q_x, q_z) = \frac{L_x L_y}{q_z^2} \sum_{i,j}^{N} \Delta\rho^2 \mathrm{e}^{-q_z^2\sigma_i\sigma_j} \mathrm{e}^{-\mathrm{i}q_z(h_i - h_j)} \epsilon_{ij}(\mathbf{q}), \tag{3}$$

with

$$\epsilon_{ij}(\mathbf{q}) = \int \mathrm{d}r\, r(\mathrm{e}^{q_z^2 c_{ij}(r)} - 1) J_0(q_r r), \tag{4}$$

where $\Delta\rho$ is the effective scattering length contrast between the bilayer and water. In a more general expression, the whole scattering length profile across one lamellar unit of length d is accounted for by a multiplicative formfactor. $L_x L_y$ is the illuminated area.

If the diffuse scattering is integrated over the direction perpendicular to the plane of incidence (hence over q_y), the term $J_0(q_r r)$ in the integral has to be replaced by $\cos(q_x r)$. By insertion of modelled or derived functions $g_{ij}(r)$ in equation (4), the scattering distribution can be calculated. In the following, we mainly consider two characteristic quantities:

(i) The cross-correlation length $\xi_z(q_r)$ defining the length scale over which a thermal mode is correlated as a function of the corresponding wavevector q_r, and
(ii) the decay of the q_z-integrated diffuse scattering with q_r, i.e. the structure factor of the fluctuations.

The cross-correlation function and the parameter ξ_z can be deduced from the peak lineshape and width (HWHM) along q_z. A Lorentzian lineshape indicates an exponential decrease of the cross-correlations along z with a characteristic length scale $\xi_z = 1/\mathrm{HWHM}$. Since the HWHM increases with q_r, ξ_z depends on the wavevector of the height fluctuations, or conversely, the lateral length scale of the fluctuation. Linear smectic elasticity predicts $\xi_z = 1/(q_r^2\Lambda)$.

An easy way to derive the relationship $\xi_z = 1/(\Lambda q_r^2)$ is to consider the elastic response of the multilamellar stack to the given perturbation of one bilayer. The perturbation is relaxed in the neighbouring bilayers by a combination of bending and compression modes, leading to an extended distortion field. Assuming a sinosoidal profile, the associated distortion field can be written as $u = u_0 \exp(-|z - z_0|\Lambda q_r^2) \cos(q_r r)$ with a damping length $(\Lambda q_r^2)^{-1}$ along z. Recently, this definition of Λ served as the basis of an experiment on multilamellar DMPC deposited on a surface grating [49]. At a temperature of 45 °C and an osmotic pressure of about 1.8×10^5 Pa obtained by immersing the sample in a solution of 14.2 wt% polyethyleneglycol (PEG 20000) in D_2O (corresponding to a spacing of $d = 56.3$ Å), a smectic length $\Lambda = \sqrt{K/B} = (12.4 \pm 0.7)$ Å was obtained. In this way, the elastic response can be measured, independent of thermal undulations which are quite weak in stiff membrane systems and therefore difficult to characterize experimentally. In smectic systems, static topological defects lead to deformation fields, which may lead to amplitudes comparable to thermal fluctuations [14]. The deformation fields around static defects and their influence on the peak lineshapes has been investigated [50–53].

3.1. Limits and validity of the linear model

Gouliaev and Nagle have compared the harmonic theory of bilayer fluctuations to a Monte Carlo simulation of stacks with periodic boundary conditions employing realistic (non-harmonic) inter-bilayer potentials [54]. The vertical cross-correlations in the stack were found to agree fairly well, so that the linear approximation of the inter-bilayer potential inherent in the linear model seems to be justified. The Monte Carlo simulation has been run with periodic boundary conditions. It would be interesting to run the simulations under the boundary condition of a flat substrate, to investigate the effect of the substrate on the correlation functions. In the linear smectic model, only the mean potential calculated from the (average) bilayer position enters the force balance. In other words, it is assumed that the fluctuations themselves have a negligible effect on the potential. This is related to the assumption that the Helfrich forces are negligible or small. This simplification could be eliminated in the future by generalization

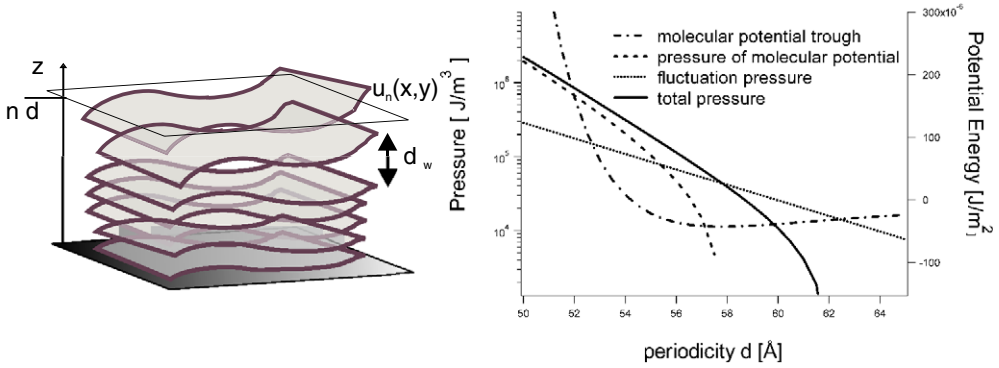

Figure 4. (a) Schematic of correlated membrane undulations causing diffuse (non-specular) scattering. (b) Pressure contributions (left axis) and molecular interaction potential (right axis) (potential trough) for DMPC as a function of the lamellar repeat distance d at zero osmotic pressure, according to the approach by Petrache *et al* [7] (see text). The solid line corresponding to the net pressure can account for the experimental $\Pi(d)$ values.

of a recent self-consistent calculation for bilayer fluctuations and interactions [55] to the case of several membranes or by use of the approach developed in [56]. Nonlinear terms in the Hamiltonian are a different issue, which also needs to be addressed [57, 56]. To elucidate the validity of the linearized model *a posteriori*, the rms deviation $\sqrt{\langle (u_n - u_{n+1})^2 \rangle}$ between neighbouring membranes can be compared to the width of the inter-bilayer potential well; see figure 4. In [58] for $N = 16$ DMPC membranes and $\eta = 0.08$ (full hydration), the bilayers in the centre of the stack were found to exhibit considerable next neighbour distance fluctuations in the range of 4–5 Å, when compared to the water layer thickness. Thus the errors made in the simplifying assumptions are probably not negligible. We note, however, that at least under high osmotic pressure, where fluctuations are small, both the mean field approach and the harmonic approximation for the potential should hold. Simulations may shed some light on these issues. To this end, membranes with fluctuating topology have been investigated by Gompper and Kroll in the vicinity of the sponge-to-lamellar transition [59], somewhat removed in parameter space from relatively stiff phospholipid membranes. For a single coarse-grained model of a bilayer Goetz, Gompper and Lipowsky have studied the transition from a collective undulations to the discrete molecular motions by molecular dynamics (MD) [60]. The first reliable fully atomistic simulation was achieved in 1993 of a lipid bilayer–water system with 200 lipid molecules or about 27 000 atoms including water [22]. More recently, full atomistic simulations of a bilayer patch have been carried out by Böckmann and Grubmüller, which are large enough in time and space to show the molecular origin of undulation modes [61]. To our knowledge, fully atomistic simulations of interacting bilayers have not yet been performed.

4. Interaction potentials

The molecular interactions for neutral lipids can be computed from the repulsive hydration and the attractive van der Waals interaction. The hydration potential is usually empirically described by an exponential function of the water layer thickness d_w [62, 63]:

$$f_{\mathrm{hyd}}(d_w) = H_0 \exp(-d_w/l). \tag{5}$$

The first derivation of this repulsion was based on a Landau free-energy gradient expansion [64], with the order parameter given by the local water polarization, which is perturbed from its bulk

value near the polar interface. The theory of hydration forces was later generalized to account for the changes observed in the decay length l with the structure of the interface [65, 66]. An alternative explanation for the hydration repulsion is based on the steric forces due to vertical motion of lipid molecules in the bilayer (protrusion forces) [67]. A discussion or even compilation of the work on hydration forces, let alone on van der Waals (vdW) forces, is beyond the scope of this article. The situation for the vdW interaction is complicated by the fact that several functional forms for this interaction potential are used in the literature to describe attraction between quasi-planar bilayers, at different levels of approximation. While waiting for an announced new textbook by Parsegian on the subject [68], the classical book of Derjaguin, Churajev, and Muller may serve as a reference [69].

Fenzl has evaluated and compared the expressions derived by Parsegian and Ninham [70] for the vdW attraction between layered materials across a gap, applicable to quasi-planar lipid bilayers [71]. Following this treatment, the interaction free energy is calculated across a planar gap d_h, composed of water and hydrophilic headgroups, which are regarded as part of the water layer separating quasi-parallel slabs of the hydrophobic chains,

$$F_\mathrm{vdW}(d_\mathrm{h}, T) = \frac{k_\mathrm{B}T}{8\pi d_\mathrm{h}^2} \sum_{n=0}^{\infty\prime} \int_{r_n}^{\infty} \mathrm{d}x\, x \ln\left[1 - \left(\frac{\Delta_n(1-\exp(-ax/d_\mathrm{h}))}{1-\Delta_n^2\exp(-ax/d_\mathrm{h})}\right)^2 \exp(-x)\right], \tag{6}$$

where d_h is the thickness of the hydrophilic layers consisting of the water layer and the headgroups and $\Delta_n = (\epsilon_{H_2O}(\omega_n) - \epsilon_{CH_2}(\omega_n))/(\epsilon_{H_2O}(\omega_n) + \epsilon_{CH_2}(\omega_n))$ is a function of the frequency-dependent dielectric constants of hydrocarbon and water. The prime symbol $'$ indicates that the static term ($n = 0$) has to be multiplied by $1/2$. The calculation is somewhat involved; however, Fenzl has shown that a frequently used approximation,

$$V_\mathrm{dis}(d_\mathrm{h}) = \frac{H_\mathrm{dis}k_\mathrm{B}T}{16\pi d_\mathrm{h}^2}\left[1 - \frac{2}{(1+a/d_\mathrm{h})^2} + \frac{1}{(1+2a/d_\mathrm{h})^2}\right] \tag{7}$$

is valid only for the dispersion term, and not for the static term which dominates under salt-free conditions. For water $\epsilon_{H_2O}(0) = 80$ and for hydrocarbon (tetradecane) $\epsilon_{CH_2}(0) = 2$ can be assumed.

Another vdW formula which is commonly used [72] uses a different partitioning of the hydrophilic and hydrophobic slabs

$$V_\mathrm{vdW}(d_\mathrm{w}) = \frac{H_\mathrm{vdW}}{16\pi}\left[1/d_\mathrm{w}^2 - \frac{2}{(d_\mathrm{w}+d_\mathrm{B})^2} + \frac{1}{(d_\mathrm{w}+2d_\mathrm{B})^2}\right], \tag{8}$$

where d_w is the water layer and $d_\mathrm{B} = d - d_\mathrm{w}$ the bilayer thickness. Of course, equation (8) and (7) are identical for $d_\mathrm{w} = d_\mathrm{h}$. If not, the difference can be partly minimized by the choice of the Hamaker constant, but always becomes large close to the singularity $d_\mathrm{w} \simeq 0$. It is clear that the expressions equations (7) or (8) should both be regarded as approximations to equations (6). In [73] (6) has been used for the static contribution[1] and equation (7) for the dispersion term with the hydrophobic bilayer thickness $a = 26$ Å and a Hamaker constant $H_\mathrm{dis} = 0.297$. The latter value has been chosen to approximate (6), evaluated for dispersion relations $\epsilon_{H_2O}(\omega)$ and $\epsilon_{CH_2}(\omega)$ which have been parametrized by oscillator models as in [71]. The total pressure derived from the combination of this vdW treatment (without free parameters) and the hydration repulsion with parameters $H_0 = 4.8\, k_\mathrm{B}T/\text{Å}^2$ and $l = 1.88$ Å, can almost alone account for the

[1] In [73] the static part for $n = 0$ was numerically integrated between 0 and 100. For water $\epsilon_{H_2O}(0) = 80$ and for hydrocarbon (tetradecane) $\epsilon_{CH_2}(0) = 2$ was taken.

experimental pressure curve $\Pi(d)$ of DMPC. However, a 10% reduction of the vdW attraction potential was needed to obtain good agreement [73]. The finding of a 'weaker' attractive force than expected may be an artificial effect originating from neglecting the fluctuation repulsion (steric Helfrich forces).

Steric forces between undulating bilayers were introduced long ago by Helfrich. Experimentally, the dominant role of steric undulation repulsion is well established in swollen phases of non-ionic surfactants, which are known to be stabilized by steric repulsion. Petrache *et al* [72] have discussed the relevance of Helfrich forces for neutral phospholpid membranes, and also the problems involved in finding the right expression for the steric repulsion force, from an experimental point of view. In the literature, the expression

$$f_{U1} = 0.42\frac{(k_{\mathrm{B}}T)^2}{\kappa d_{\mathrm{w}}^2}, \tag{9}$$

for the undulation force was derived by Helfrich for the so-called hard confinement regime (e.g. a single membrane in between hard walls). Later it was been argued that the case of *soft confinement*, i.e. a membrane in between neighbouring lamellae, should be better described by very different functional dependence, namely

$$f_{U2} = \frac{(\pi k_{\mathrm{B}}T)}{16}\frac{H_0}{\kappa\lambda^2}\exp(-d_{\mathrm{w}}/(2\lambda)). \tag{10}$$

Apart from the important question of which functional dependence is applicable, the question of the exact numerical prefactor e.g. in (9) is also under debate. More importantly, it has been shown that the undulation repulsion cannot be simply added to the molecular forces, but must be treated by field theoretical approaches which go beyond the mean field approximation [74], or by self-consistent models [55], but which to date have not been combined with realistic molecular potentials and multilamellar stacks. Facing these complications, Petrache and co-workers [72] have pointed out that the measured rms fluctuation of the next neighbour distance $\sigma = \sqrt{\eta}d/\pi$ can be used to determine the fluctuation pressure P_{fluct} experimentally, which is then added to the pressure calculated from the molecular potentials to fit the data $\Pi(d) = P_{\mathrm{mol}} + P_{\mathrm{fluct}}$. To this end, they derived the formula $P_{\mathrm{fluct}} = -\frac{(4\ k_{\mathrm{B}}T)^2}{(8\pi)^2} \sim \frac{1}{k} \sim \frac{\mathrm{d}\sigma^{-2}}{\mathrm{d}d_{\mathrm{w}}}$. A typical curve for the fluctuation pressure is shown in figure 4. The values are close to those obtained from the σ values measured in aligned DMPC membranes (oligo membranes) by Mennicke *et al* [58, 73] as a function of osmotic pressure. Note that this study reports a very similar $\Pi(d)$ curve as in the bulk case [7]. Therefore, the bulk and thin film case can obviously be treated with essentially the same interaction potentials.

The results obtained by the approach of Petrache *et al* are illustrated in figure 4. The different pressure contributions from the molecular interactions (hydration plus vdW) and the fluctuation pressure (see above), as well as the total pressure, are plotted as a function of d (left axis), along with the bare molecular interaction potential (right axis) obtained from adding the vdW and hydration potentials, with parameters $H_0 = 0.020\ \mathrm{J\,m^{-2}}$ and $l = 1.97$ Å (hydration repulsion) and $H_{\mathrm{vdW}} = 4.91 \times 10^{-21}$ J (using equation (8)). The fluctuation pressure corresponds to that of $\kappa = 18.5\ k_{\mathrm{B}}T$. Note, however, that by a different choice of parameters the same total pressure curve $\Pi(d)$ can also be modelled with a much smaller bending rigidity (if H_0 and H_{vdW} are adjusted accordingly). Resulting from the Petrache approach, we see that the equilibrium swelling for fully hydrated DMPC is significantly higher than the equilibrium swelling expected from molecular forces alone, due to the fluctuation pressure. In her dissertation, Mennicke gives an alternative interpretation of the $\pi(d)$ curve, based only on bare molecular interactions and using the vdW formulas based on the Fenzl approach, but neglecting Helfrich steric forces. Consequently, the minimum of the molecular potential trough is now located exactly at the equilibrium swelling distance, as it must be if

no additional steric repulsion is taken into account. Note that the decomposition into different interaction contributions cannot be decided from the $\Pi(d)$ data alone. Finally, we point out that the molecular interactions yield a very asymmetric potential trough. Therefore, the parabolic approximation (linear fluctuation models) can be expected to break down as soon as the fluctuation amplitude is larger than a few ångströms.

5. Specular reflectivity

Specular x-ray (SXR) and neutron reflectivity (SNR) are used to deduce the density profiles of membranes along the interface normal. From the reflectivity curves, the laterally averaged scattering length density profile $\rho(z)$ can be derived with molecular resolution. To this end the reflectivity is measured over a large range of grazing incidence angles α_i, or correspondingly vertical momentum transfer q_z. In contrast, the lateral interface structure given by the variations of the scattering length density in the xy plane determines the non-specular scattering (NSNR) measured at angles of exit $\alpha_f \neq \alpha_i$ [46, 75], as discussed in the next section. Figure 5 shows a typical reflectivity curve measured on a thick multilamellar stack, along with the resulting density profile on an absolute scale of electrons per volume. A necessary condition is a clear distinction between specular and non-specular scattering components. Data analysis and modelling is based on the fully dynamical Parratt algorithm (taking into account multiple reflections) or alternatively on the semi-kinematical reflectivity pioneered by Als-Nielsen [21]. The observation of a region of total external reflection and hence of the critical angle α_c allows for the determination of the scattering length density profile on an absolute scale. The full q_z-range can be used for data analysis by fitting the reflectivity curve to a parametrized model of the density profile [76]. The highest q_z values of the curve limit the achievable spatial resolution in $\rho(z)$. Note that the advantage of full q_z-fitting has also been demonstrated in bulk (SAXS) studies; see for example [77]. In most studies of oriented bilayers, however, only the integrated Bragg peaks of the multilamellar samples are used for data analysis, and the one-dimensional density profile $\rho(z)$ is computed by Fourier synthesis using a discrete set of Fourier coefficients f_n as described in [78, 12]. In this approach, the exact relation between Bragg peak intensity and the Fourier coefficients f_n is problematic [79], since the scattering contributions of specular and non-specular scattering are governed by a different q_z dependence. Taking into account effects of absorption, polarization, specular and non-specular Fresnel reflectivity components, illumination correction, etc, a widely used correction factor is $I_n = |f_n|^2/q_z$, where q_z^{-1} is termed a Lorentz factor for oriented bilayers.

In an attempt to go beyond the Fourier synthesis approach, we have recently employed a reflectivity model in the framework of semi-kinematical scattering theory, in which both the structure factor of the stack and the bilayer form factor are suitably chosen [76], according to the resolution of the experiment. The starting point for this model is the so-called master equation of reflectivity from a structured interface in the semi-kinematic approximation [21]. The reflectivity from an interface with its normal along z is determined by the scattering length density profile $\rho(z)$ between a medium 1 (air or water) with scattering length density ρ_1 and a medium 2 (solid substrate) with density ρ_2, and can be written as

$$R(q_z) = R_F(q_z)\,|\Phi(q_z)|^2 = R_F(q_z)\left|\frac{1}{\Delta\rho_{12}}\int \frac{\partial\rho_e(z)}{\partial z} e^{-iq_z z}\,dz\right|^2, \qquad (11)$$

where R_F is the Fresnel reflectivity of the ideal (sharp) interface between the two media, and $\Delta\rho_{12}$ is the scattering length density contrast. Note that ρ is obtained by the combination of the solid surface and a step train of lipid bilayers, convolved with a function describing the positional fluctuations and multiplied by a coverage function; see below. The critical

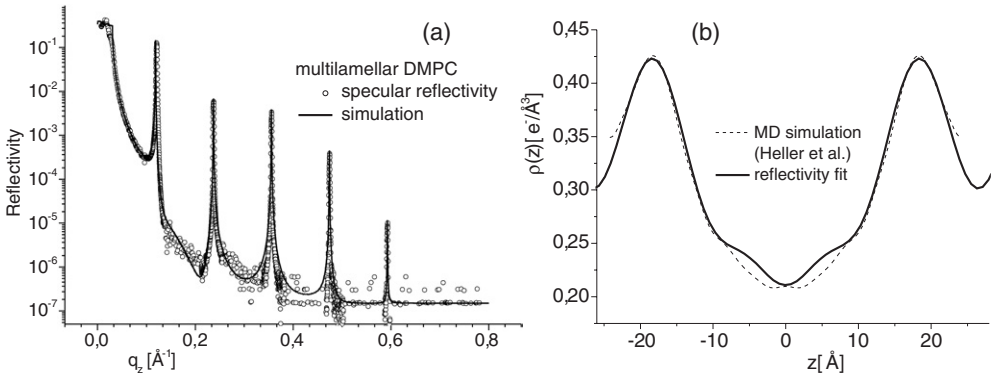

Figure 5. (a) Multilamellar reflectivity curve with sharp Bragg peaks (symbols) in the fluid phase, shown for OPPC at partial hydration, along with a least-squares fit (solid curve). (b) Density profile corresponding to the fit shown in (a), compared to MD simulation results [22] (dashed curve). From [76].

momentum transfer or the critical angle in R_F is directly related to the density contrast by $q_z = 4\pi/\lambda \sin(\alpha_c) \simeq 4\sqrt{\pi \Delta\rho_{12}}$. Absorption can be accounted for by an imaginary component of the wavevector. The bilayer form factor $F(q_z)$ is parametrized by variable number N of Fourier coefficients taken to describe the model density profile $\rho(z)$, where N is adapted to the resolution of the measurement. In contrast to conventional box models, the total number of parameters can thus be kept small, while still fitting to reasonable density profiles. The number of n Fourier coefficients can easily be changed by way of a linear transformation into a parametrization of n (independent) structural parameters of the bilayer, such as bilayer thickness (headgroup peak-to-peak), density maximum in the headgroup maximum, density in the bilayer centre plane, density of the water layer, etc. As a test example, the reflectivity of highly aligned multilamellar 1,2-oleoyl-palmitoyl-sn-glycero-3-phosphocholine (OPPC) membranes on solid substrates has been measured and analysed; see figure 5. The density profile agrees remarkably well with the bilayer structure as obtained from published molecular dynamics (MD) simulations [22], without free scaling parameters [80]. In a second step, the model was generalized to account for thermal and static defects. The reflectivity structure factor depends on the precise form of the function $\sigma(n)$, where σ is the rms amplitude of thermal fluctuations which increases with n from the flat substrate to the top of the film [44]. In addition, a decreasing coverage function has been implemented [44, 58], accounting for non-uniform film structure due to domains. The domain structure may result from the non-equilibrium deposition process and/or equilibrium wetting properties [27]. The fits obtained from the model give very satisfactory results and describe the data well over the whole range. Accordingly, several structural and interaction parameters can be extracted. The fitting routine has been applied on oligo-membranes of DMPC to determine the inter-bilayer potentials of DMPC as a function of osmotic pressure, imposed by a neutral polymer solution [58].

Finally, we give an example of single bilayer reflectivity. Figure 7 shows a DMPC reflectivity curve corresponding to a single bilayer remaining after thermal unbinding. Instead of multilamellar Bragg peaks, a smooth and broad modulation of the Fresnel reflectivity $R_F(q_z)$ is observed. The modulated intensity decay is highlighted by dividing out the Fresnel term $R_F(q_Z)$. Again, the curve is analysed by the semi-kinematical model. Parameters of inter-bilayer fluctuations do not enter single bilayers, and only a form factor has to be specified, simplifying the analysis. The example shows that the unbinding pathway can be used to

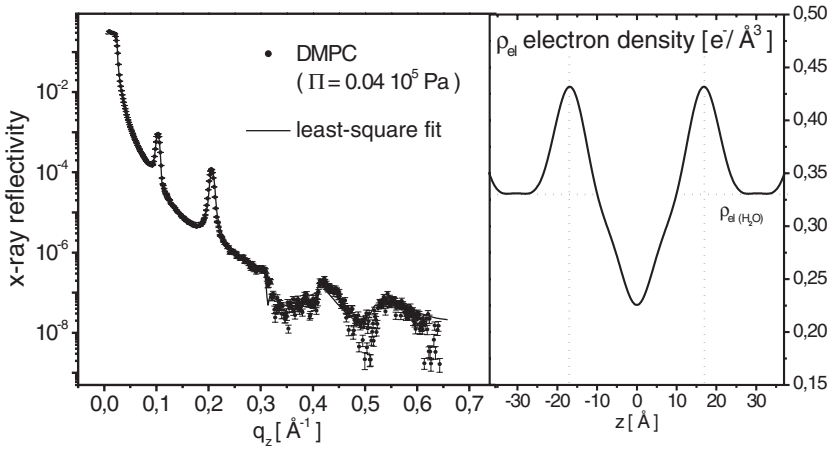

Figure 6. Left, measured reflectivity curve (symbols) of a stack of about 16 DMPC membranes in the fluid L_α phase on silicon substrates at an osmotic pressure of 0.04×10^5 Pa imposed by a polymer stressor in solution. The least-squares fit (solid curve) to the kinematic reflectivity model describes the whole curve quantitatively including the higher orders which become deformed by the presence of thermal fluctuations. Note that the corresponding density profile (right) is obtained on an absolute scale without free scaling parameters. From [58].

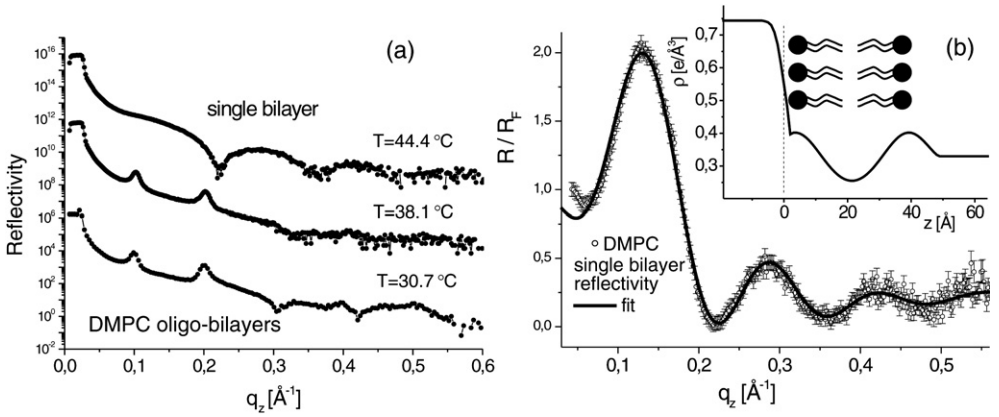

Figure 7. (a) DMPC reflectivity curves of oligo-membranes prepared by spin-coating. Between $T = 38$ and 44 °C the membranes unbind from the surface except for one single bilayer remaining attached to the silicon surface (upper curve). Data taken at D4/HASYLAB, as described in [73]. In (b) the single bilayer curve with its characteristic reflectivity oscillations is shown after division by the Fresnel reflectivity, along with a least-squares fit. The corresponding density profile is shown as an inset.

prepare a single bilayer. Single bilayers adsorbed to the solid substrate are known to exhibit different structure and properties (e.g. fluidity) than a free bilayer. Novel methods to prepare double bilayers or free floating bilayers have therefore attracted much attention [17]. These systems have also been employed to study the anomalous swelling observed at the main phase transition of DMPC, DLPC and other phospholipids [81].

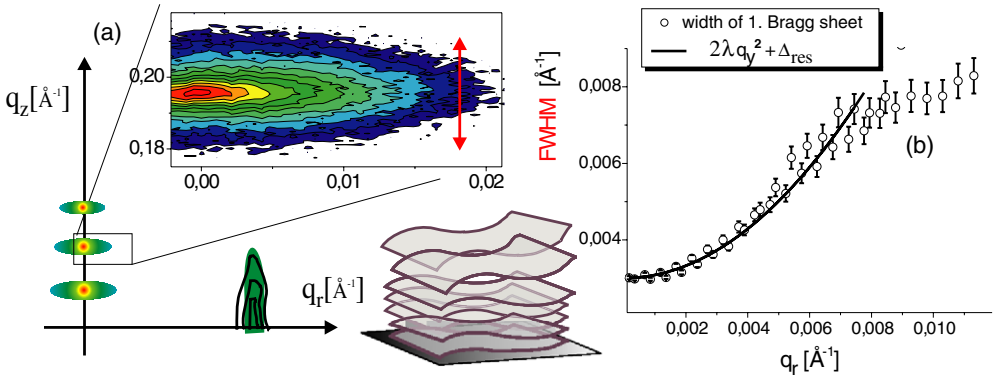

Figure 8. (a) Typical diffuse scattering distribution of multilamellar lipid bilayers (DMPC, fluid phase). The fluctuations lead to the lateral extension of the diffuse scattering around the Bragg positions. The vertical correlation of the bilayer undulation (conformality) defines the width of these 'Bragg sheets' along q_z. (b) Increase in the width (vertical q_z-width) of the first Bragg sheet as a function of lateral momentum transfer. The parabola indicates a regime which follows the linear smectic model. The coefficient of the parabola gives the smectic length scale Λ.

6. Non-specular (diffuse) reflectivity

Specular and diffuse (nonspecular) x-ray (NSXR) and neutron reflectivity (NSNR) yield model independent information on the height–height correlation functions [14, 38]. The nonspecular (diffuse) intensity distribution can be described by a structure factor $S(q_z, q_r)$, measured as a function of the parallel and vertical components of the momentum transfer, $q_r = \sqrt{q_x^2 + q_y^2}$ and q_z, respectively. As an example, figure 8 shows the diffuse intensity of the second Bragg sheet for a sample of several hundred DMPC bilayers in the fluid phase. Data were taken at the undulator beamline ID1 of ESRF (European Synchrotron Radiation Facility) in Grenoble, using a collimated x-ray beam of 20 keV photons to traverse the 18 mm of bulk water in the temperature-controlled chamber [82], at constant angle of incidence. Note that in the case of vanishing fluctuations intensity would be observed only at the specular position! The diffuse sheet arises from the vertical correlations of the bilayer undulations. Correspondingly, the q_z profiles of the diffuse Bragg sheets carry the information on the height–height cross-correlations. The Lorentzian lineshape along q_z indicates an exponential decrease of the cross-correlations along z with a characteristic length scale $2/\mathrm{FWHM}$. The FWHM increases with q_r, reflecting a strong dependence of the cross-correlation length on the wavenumber q_r. Smectic elasticity predicts $\mathrm{FWHM} = 2\Lambda q_r^2$. Figure 8(b) shows values obtained at the $n = 1$ Bragg sheet (DMPC, $T = 41.82\,^{\circ}\mathrm{C}$). The least-squares fit to $\mathrm{FWHM} = 2\Lambda\, q_r^2 + \Delta_{\mathrm{res}}$ (solid curve) shows the range over which the linear model describes the data well. Δ_{res} accounts for the instrumental resolution. Unfortunately, the nonlinear relation between g_{ij} and $S(q_r, q_z)$ introduces a systematic increase of the measured value Λ with n, so that the 'true' parameter Λ should be determined from extrapolation to small $q_z\sigma \leqslant 1$. Depending on the fluctuation amplitude, this condition may be fulfilled at the first Bragg sheet $n = 1$, but often is not for the higher orders.

Horizontal slices, e.g. slices along q_r, are evaluated to quantify the decay of the diffuse scattering with q_r for $n = 1, 2$. The integration in q_z (corresponding to the vertical width of the slice) can be increased to approximately cover one Brillouin zone $\pm\pi/d$. In this case, it can be shown that the contributions of the cross-correlation terms $i \neq j$ cancel, and one is left with a

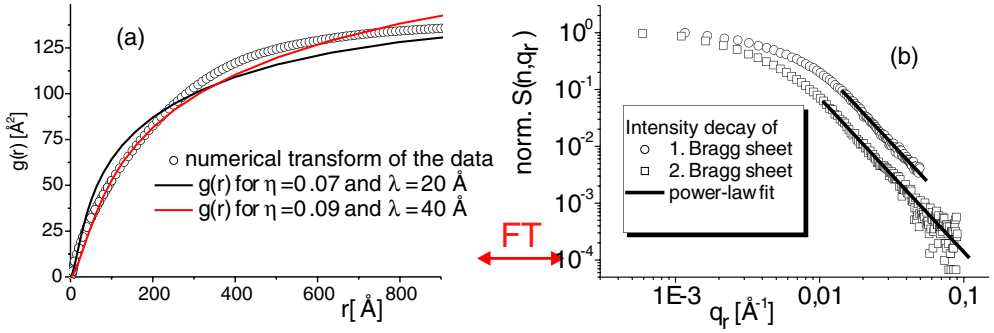

Figure 9. (a) Characteristic height–height self-correlation function of an averaged membrane in the stack as derived from the data, together with theoretic function (see text). (b) Decay of the (q_z-) integrated intensity of the first two Bragg sheets $n = 1$ and 2. Note that (a) can be obtained from a transformation of the curves in (b) and proper normalization.

curve which corresponds to the transform of an average height–height self-correlation function $g(r)$ [48]. The data thus correspond to the averaged structure factor $S(n, q_r)$ of a bilayer in the stack, measured at the order n. In the limit of small $q_z\sigma$ the curves should overlap for all orders n and be proportional to the bilayer power spectral density (PSD). Again, a systematic shift with n is observed due to the nonlinearity in equation (4). Figure 9(a) shows the decay of the integrated intensity with q_r for $n = 1, 2$, respectively, for DMPC at $T = 41.8\,^{\circ}\mathrm{C}$. At small q_r a plateau is observed, while at high q_r a power law behaviour $S(q_r) \propto q_r^{-\gamma}$ is observed, with $\gamma = 2.71 \pm 0.03$ for the first, and $\gamma = 2.70 \pm 0.03$ for the second Bragg sheet, respectively. This is in striking contrast to the $\gamma = 2 - \eta$ behaviour expected for a simple logarithmic correlation function $g(r)$ according to linear smectic elasticity theory (continuum model) [83], and also in contrast to an asymptotic $\gamma = 4$ power-law, which is the prediction of the discrete smectic model for high q_r. Correspondingly, the smectic correlation functions do not quantitatively describe the experimental real-space correlation function $g_{\mathrm{exp}}(r)$, as obtained by the numerical back-transformation (inversion) of the experimental data presented, see figure 9. $g_{\mathrm{exp}}(r)$ can be directly computed from a numerical back-transformation of the experimental data [14].

We must also keep in mind that the theoretic form is derived for infinite bulk samples, while the experimental function saturates at a value of $2\sigma^2$ for $r \geqslant \xi_{\mathrm{max}}$, due to finite D. The expression for $g(r)$ obtained for flat surface boundary conditions should therefore better be compared to the model by Constantin *et al* derived for this case [44]. However, this does not completely remove the discrepancies. $g(r)$ can be scaled against g_{exp} by variation of the parameters B and K to give qualitative agreement. Note, however, that the parameters also have to conform to the $\Lambda = \sqrt{K/B}$ values determined from the analysis of the Bragg sheet width, so that there is only one 'free' parameter. We stress that not just in the analysis of $g_{\mathrm{exp}}(r)$, but already on the level of the raw data, discrepancies from the expected behaviour are observed. In particular, the asymptotic power-law behaviour of the experimental curve $g(r) \propto r^{0.7}$ (or the *roughness exponent*) is notably different from the smectic model, which predicts a crossover from $g(r) \propto r^2$ (discrete Hamiltonian) to a logarithmic form. At the same time, the quadratic increase in the peak width (HWHM in q_z) saturates at $q_r \geqslant 0.01\ \mathrm{Å}^{-1}$, also indicating that at the corresponding small lateral distances the linear smectic model does not completely describe the data. Therefore, the applicability of the Caille model must be questioned even if for selected parameters $K = \kappa/d$ and B or equivalently Λ and η a reasonable scaling can be obtained for $g(r)$. In the original letter we hypothetically invoked contributions from non-bending modes in the diffuse scattering. This conclusion was based on the fact that in [48] the main discrepancies

were initially observed at small r. Unfortunately, however, this comparison was flawed by a numerical error in the calculation of the theoretic function [84]. The corrected curves do not show particular discrepancies at small r. Partial agreement can be obtained, but depending on where agreement is sought these effective values can be shifted. Whether the persisting discrepancies are due to other collective modes than bending modes (as speculated in [48]), a q_r-dependence on κ, or nonlinear terms has to be decided by future studies. We stress that the approach discussed above is model independent, since we do not assume a specific model first, but are able to determine the correlation functions directly, which are then compared to theory in a second step.

Regardless of the remaining inconsistencies between model and data, one tendency is clear: κ comes out much smaller than expected. The simulation with $\eta = 0.07$ and $\lambda = 20$ Å corresponds to $\kappa \simeq 7\ k_B T$ and the simulation with $\eta = 0.09$ and $\lambda = 40$ Å corresponds to $\kappa \simeq 11\ k_B T$; see figure 9 for a curve measured at $T = 41.8\,^{\circ}$C. This range of κ can be compared with a recent measurement of $\Lambda = 12.4$ Å at $T = T = 45^{\circ}$ obtained from DMPC membranes deposited on surface gratings [49], which at an osmotic pressure corresponding to $B = 4.5$ MJ m^{-3} (DMPC, $d = 56$ Å) yields a bending stiffness of $\kappa = 9.7\ k_B T$.

As a function of T [48], $\kappa(T)$ was found to stay approximately constant over the whole range of T in the fluid phase except for a small decrease in the vicinity of the main phase transition $T \simeq 23.5\,^{\circ}$C. B was found to increase steeply at the transition to the gel phase. Note, however, that the resolution in T was not good enough to investigate effects linked to the anomalous swelling behaviour just above the transition, in the range where Chu *et al* recently found a reduction in B [85]. On a wider scale of temperatures in the fluid phase B was found to decrease linearly, indicating a corresponding softening of the inter-bilayer potential with T. Extrapolating the linear regime to high T, B would vanish around $T \simeq 110\,^{\circ}$C. The decrease in B may be linked to the previously observed transition from a bound state to an unbound state, where the multilamellar membranes detach from the substrate and get dispersed into the aqueous bulk [29, 86]. As a precursor effect to this transition, the inter-bilayer potential $f(d)$ appears to soften, resulting in a shallower minimum.

Compared to the above results, most values reported in the literature for κ are higher. An x-ray lineshape study on bulk suspensions gave $\kappa = 13.4\ k_B T$ [87], in good agreement with micropipette aspiration results [88]. Another study on bulk DMPC employing full q-range fits and osmotic pressure variation reports $\kappa = 11.5\ k_B T$ [89], again at full hydration and comparable T. More recently, Chu *et al* have investigated the softening of κ in the vicinity of the main transition temperature, associated with the anomalous swelling behaviour. For $T = 30\,^{\circ}$C, well above the anomalous swelling regime, they report $\kappa \simeq 16\ k_B T$ for DMPC [85]. These latest results have been obtained by a method first reported in [15] to extract the structural and fluctuation parameters of solid-supported bilayers. In contrast to the approach discussed above, the data are collected on samples deposited on curved substrates. The diffuse scattering is mapped by a CCD detector. Each pixel collects diffuse scattering corresponding to different angles of incidence and exit. The decay of intensity with q_y at different q_z is then plotted and fitted to the bulk smectic model [90, 85]. The authors quantified the decrease of κ (softening) when approaching the transition temperature, in a range which was not resolved in the study of [48]. The difference from the results reported here from Bragg sheet analysis remains unclear. The variation of reported values of the elasticity parameters in the literature may be taken as an indication that B and K are indeed effective parameters. While experiments are limited by their respective windows of length scale and resolution, but also the linear model may be limited in its capability to describe all of the data consistently.

In deducing elasticity parameters from scattering results, two different levels should be separated: on the first level, the x-ray scattering results are structural quantities. On the second

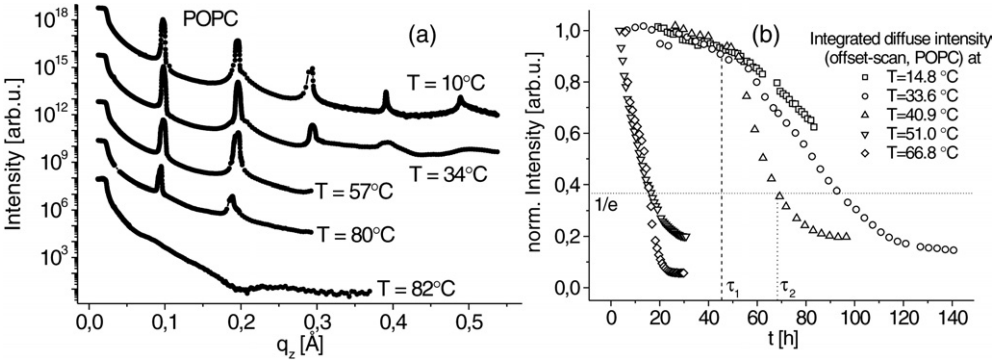

Figure 10. (a) Typical temperature-dependent reflectivity for a solid-supported lipid stack (OPPC). Upon increase of T the higher orders decrease. No strong swelling is observed, i.e. the changes in d are on the order of a few per cent. Moreover, at some temperature T_u (depending on heating rate, waiting time and sample thickness), a complete unbinding of the stack is observed, with one single bilayer remaining on the substrate. (b) Kinetics of unbinding at constant T, as obtained by plotting the diffuse intensity which is proportional to sample volume as a function of t. From [91].

level, the transformation of this structural data to elasticity parameters is another issue, and is necessarily model dependent. Specific assumptions which have to be made in the calculation of κ are the following. (i) Vanishing surface tension at the film/water interface and negligible lateral tension induced by defects or domain edges. (ii) Only the mean potential calculated from the (average) bilayer position is relevant for the force balance. This simplification could be overcome in the future by generalization of a recent self-consistent calculation for bilayer fluctuations and interactions [55] to the case of several membranes or by use of the approach developed in [56]. (iii) Vanishing non-linear effects due to the asymmetry of the potential. Again, this limitation could be overcome by more general models [57, 56] and/or numeric simulations. To elucidate the validity of the linearized model *a posteriori*, the rms deviation $\sqrt{\langle (u_n - u_{n+1})^2 \rangle}$ between neighbouring membranes can be compared to the width of the inter-bilayer potential well; see figure 4(b). For $N = 16$ and $\eta = 0.08$ (full hydration) the bilayers in the centre of the stack were found to exhibit considerable next neighbour distance fluctuations in the range of 4–5 Å, when compared to the water layer thickness [58]. Thus the errors made in the simplifying assumptions are probably not negligible. In order to shed more light on this, not only static properties but also temporal (dynamic) properties of the undulation should be probed in the future, e.g. by inelastic scattering or photon correlation spectroscopy, which have proven successful in studies of thermotropic smectic films [8].

7. Thermal stability and unbinding

Highly oriented lipid films on solid surfaces can be studied while immersed in excess water [32, 29]. In this set-up, a thermal transition was observed [29], from a substrate bound, multilamellar state at low temperatures to a state of freely dispersed bilayers in water at high temperatures. The transition was first observed at around 80 °C for oleoyl-palmitoyl-sn-glycero-phosphocholine (OPPC) and 95 °C for dimyristoyl-sn-glycero-phosphocholine (DMPC), and was not accompanied by an observable regime of critical swelling (no significant shift in peak position), but by pronounced precursor effects in the lineshape of the multilamellar peaks. Figure 10(a) shows a typical T-dependent reflectivity curve for a multilamellar stack

of OPPC. Later it became clear that the transition temperature depends on the thermal history of the sample, and strongly varies with the rate of heating, pointing at strong kinetic effects, once the films are heated up close to the transition [91, 86]. In some cases, even at room temperature, lipid membranes eventually unbound after waiting long enough (on the order of hours to days). In very thin preparations of about ten bilayers, unbinding occurs at significantly lower temperatures than in thick samples, where the number of bilayers is typically on the order of a few hundred. A single membrane was found to remain on the substrate, also at high temperatures close to the boiling point [92, 91]. In some cases, small patches of multilamellar stacks may still stick to the surface. Figure 7 shows the reflectivity of a single bilayer, obtained after an unbinding cycle of oligo-DMPC bilayers. Experimentally, the single-bilayer signal is much weaker than the multilamellar one, and can sometimes be overlooked at small signal to noise. The results have been confirmed independently by fluorescence microscopy, which showed a homogenous coverage of a (dyed) lipid bilayer remaining on the substrate [91]. We denote this instability the 'experimental unbinding instability of solid-supported bilayers'. Some researchers oppose this classification to avoid confusion with the well studied theoretic models of unbinding [86]. We stress that the phenomenon is observed reproducibly; it cannot be regarded as an accidental 'loss of sample', but must be considered as an experimentally relevant instability of aligned bilayers. It is understood that the origin of the phenomenon must not necessarily be repulsive steric forces due to increased undulations, as treated theoretically by Lipowsky and co-workers [93].

Experimentally, the unbinding transition of solid-supported bilayers has been studied for DMPC, OPPC, DLPC, and DGDG [91]. The curves have been measured on the timescale of several hours, heating the sample up to a new temperature point after each scan. Upon heating of the sample, the higher order reflectivity peaks successively decrease in an almost universal manner, without any significant change in d. Finally, all peaks vanish, and a curve remains, characteristic for a single bilayer on a substrate; see figure 7. Up to the last step, which corresponds to the total loss of multilamellar domains, or complete unbinding, the process is largely reversible, i.e. the higher order peaks come back in intensity upon cooling. The scenario is unchanged if silicon is replaced by glass substrates. However, the actual temperature of unbinding T_u may change from one experiment to the next within some range. In fact, it is very difficult to determine T_u, since the process of unbinding is very slow. If a certain temperature is reached, the unbinding pathway may still continue with time. In other words the unbinding transition is characterized by strong kinetic effects, and it is often unclear whether a multilamellar stack is stable or metastable at a given T. Note that DMPC in the L_α phase at $T < 30\,^\circ$C has been observed to remain unchanged over four weeks in excess water. The total intensity in the reflectivity and in the (diffuse) offset scan remained unchanged, indicating that no loss of scattering volume had occurred. OPPC on the other hand slowly unbinds with time, even at small temperatures, as low as $T = 14.8\,^\circ$C. Thus, the measured value of T_u also depends the time τ over which T_u has been reached in a temperature ramp. At constant temperature T, the sample may unbind after a latency time τ or the rate of heating. The unbinding also depends on sample history. Tempering at higher temperatures reduces τ. Above all, the total number N of bilayers or equivalently the thickness D of the sample has a strong influence on τ at given T, or conversely T_u at given heating rate. The kinetic aspects of the unbinding transition are illustrated in figure 10 for thick (spread) OPPC samples. The scattering volume as determined from the integrated peak intensity has been plotted as a function of time t for a range of T. For the curves of $T > 40\,^\circ$C the curves decay monotonically and quite rapidly. A characteristic time τ can be defined from the $1/e$ value of the normalized scattering intensity, even if the decay is not always exponential. In contrast, at $T \leqslant 40\,^\circ$C the curves are first almost constant, and then decay rapidly only after some initial incubation time.

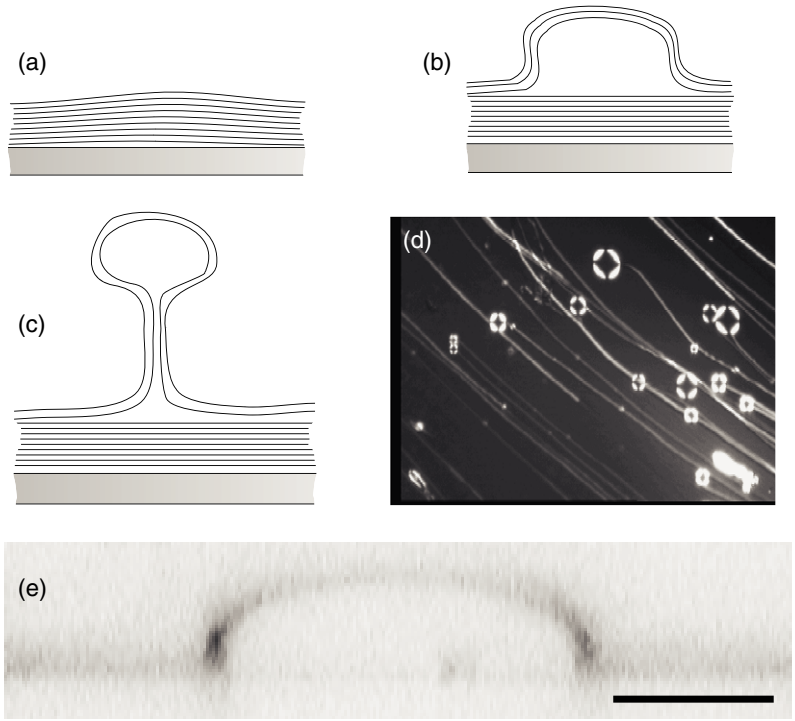

Figure 11. (a) Unbinding scenario solid-supported bilayers following from x-ray and optical microscopy studies [91]. (a)–(c) The observed transition from planar bilayers to multilamellar vesicles (MLVs). The MLVs remain partly attached to the film by a tether, as indicated by polarized optical microscopy (d), from [91]. (e) Confocal fluorescene microscopy shows that below the unbinding temperatures multilamellar 'blisters' form at the film surface, which then eventually detach at higher temperature, from [91].

The nature of the incubation process and time remains speculative. Possibly, it can be linked to mesoscopic defects, which anneal or change on the timescale of many hours, depending on the temperature. Other 'unbinding agents' than temperature have been identified. Mixing water with pentanol in the excess phase leads to unbinding of a stack of DMPC within one hour [91]. Application of a DC electric field was found to induce a similar pathway and transition from planar bilayers to vesicles [94, 95]. Finally, we note that charged bilayers were observed to unbind by salt dilution [91]. In neither case was a significant swelling observed, i.e. changes in d were on the order of a few per cent. In contrast, charged bilayers in salt free solutions balanced by osmotic pressure [33], or soft uncharged bilayer systems with strong Helfrich repulsion, exhibit significant swelling of d up to a few hundred per cent.

The unbinding phenomena discussed here for solid-supported bilayers differ from the experimental observations made in bulk suspension of lipid mixtures close to the main phase transition [96], where a discontinuous and reversible thermal unbinding was observed for charged membranes. This finding is possibly in closer relationship to the theoretic predictions than the instability in solid-supported films. The coupling of the main phase transition to critical unbinding has been discussed for some time. Experimentally, several physical membrane properties like diffusion constants, permeability, NMR order parameters, and structural parameters like multilamellar periodicity exhibit a continuous pretransitional behaviour just above the first order transition to the gel phase, e.g. at the L_α to $P_{\beta'}$ (ripple phase) transition

in DMPC and other phospholipids. Structurally, the discussion has focused on the observed continuous (critical) swelling (also termed anomalous swelling) of multilamellar membranes in the vicinity of the transition. While the observation of an increase in the lamellar periodicity $d(T)$ just above the transition was highly reproducible and undisputed, the origin of this effect was attributed to (a) a softening of the bilayer and a corresponding increase of fluctuations leading to a swelling of predominantly the water layer [97] or (b) a critical increase in the bilayer thickness δ_m [98]. It seems that the issue could not be resolved by experiments on isotropic suspensions alone. To this end, more recent experiments on highly oriented films are helping to bring a definite answer to the puzzle [99, 81, 85]. For the anomalous swelling behaviour, the experimental results converge in that the swelling takes place primarily in the water layer. In order to decide whether this is indeed an effect of steric repulsion due to bilayer softening necessitates the measurements and analysis of the diffuse scattering [85], which directly reflects the bilayer fluctuation properties near the transition, in addition to the form factor (i.e. density profile) analysis. Furthermore, elastic scattering should be completed by inelastic scattering data to elucidate the dynamical properties associated with the transitions. Recently, anomalous swelling was shown to be suppressed at high hydrodynamic pressures [100], and explained based on a coupling between the main phase transition temperature and an unbinding temperature (which is however not reached) in most systems.

8. Elastic and inelastic studies of the chain correlation peak

The structure and the dynamics of the fluid bilayer are of interest not only in the mesoscopic limit, where different bending and compressional modes are present, but also on the molecular length scales, which are relevant for many biophysical properties such as diffusion and transport. In this context, the short range ordering of hydrocarbon chains in simple phospholipid bilayers was investigated, using aligned stacks of lipid membranes. The x-ray peak associated with the hydrocarbon chains can be probed by means of a reciprocal space mapping (RSM) as a function of two coordinates, the momentum transfer parallel and perpendicular to the bilayer, over a wide range and at high resolution. Structural results can be obtained concerning the distribution of tilted segments, the correlation length, and the radial distribution function of the quasi-two-dimensional (2D) liquid structure. The fluid chains exhibit a collective dynamics, which has to be elucidated to understand key functions of a membrane [101]. The short wavelength dynamics is attributed to play a key role in the transport of small molecules through the membrane [102]. Molecular vibrations, conformational dynamics, and 'one-particle' diffusion in the plane of the bilayer can be studied by a number of different spectroscopic techniques covering a range of different timescales such as incoherent inelastic neutron scattering [103] or nuclear magnetic resonance [104]. In contrast, few experimental techniques are able to elucidate the short range collective motions mentioned above. To this end, Chen *et al* made seminal inelastic measurements in phosphocholine model membranes using inelastic x-ray scattering techniques (IXS) [105]. They could determine the dispersion relation in the gel and the fluid phase of a DLPC bilayer. As a very important result, Chen *et al* found a minimum at Q_0, the maximum of the static structure factor $S(Q)$. More recently, inelastic neutron scattering (INS) was used to study the collective dynamics of the acyl chains in lipid bilayers, using the specific advantages of INS over IXS. The main differences with respect to IXS are related to the energy–momentum relation of the neutron versus the photon probe, strongly affecting energy resolution, and accessible (Q, ω) range. Due to the dispersion relation of the neutron itself ($\sim Q^2$), the range at low Q and high ω values is difficult to access by INS.

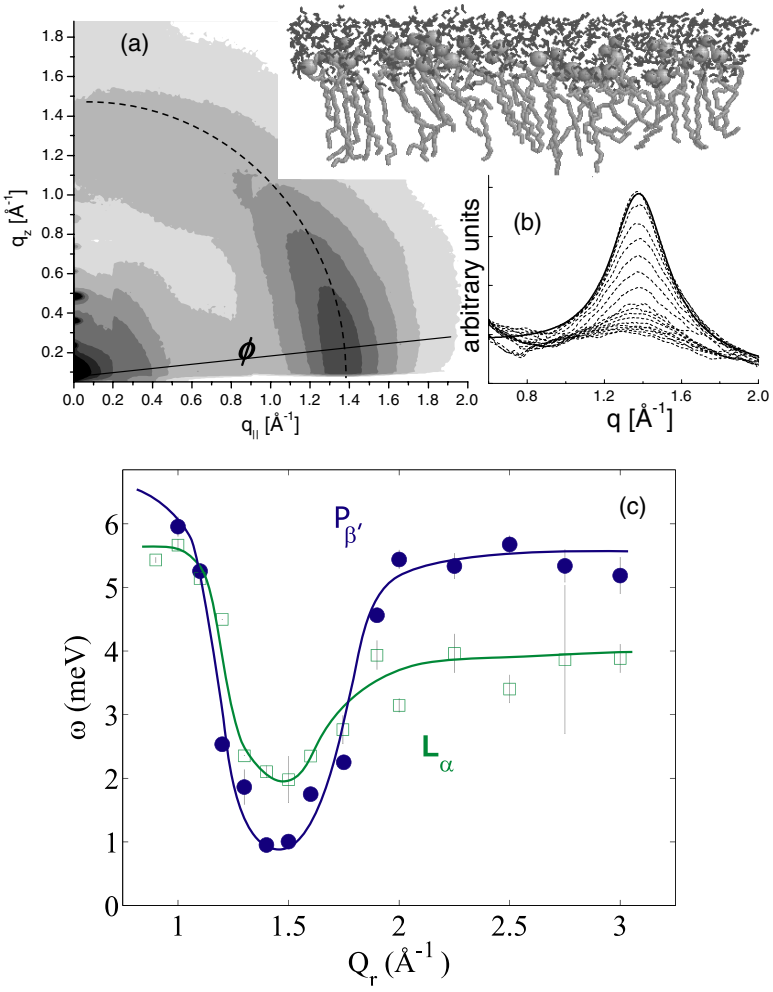

Figure 12. (a) Reciprocal space mapping (RSM) of pure POPC in the fluid L_α-phase [106]. The chain correlation peak is extended along a circle with the radius of $q \simeq 1.38$ Å^{-1}. The inset displays a configuration of chains in one half of a bilayer as obtained from MD simulations (Heller *et al* 1993). In (b) a set of radial slices (dashed) is shown, at angles ϕ ranging from $\phi = 5°$ (largest peak) to $\phi = 90°$ (lowest peak). The solid line represents a least-squares fit of the 10° slice to a Lorentzian. Adapted from [106]. (c) Dispersion relations in the gel and the fluid phase of the DMPC bilayer as obtained from inelastic neutron scattering (INS). The chain correlation maximum has been measured in energy–momentum space by several constant-Q scans at Q values ranging from $Q = 0.7$ to 3.0 Å^{-1}. Adapted from [39].

Let us briefly review some structural aspects first, as investigated in [106], and then discuss the collective dynamics, summarizing recent work by inelastic neutron scattering [107]. Figure 12(a) shows the reciprocal space mapping (RSM) of pure POPC in the fluid L_α-phase, represented in logarithmic grey shades. The chain correlation peak is stretched along a circle with radius $q = \sqrt{q_r^2 + q_z^2}$. An oblique cut through the peak at a given angle ϕ to the sample horizon shows a Lorentzian lineshape. The peak can be attributed to correlated chains with different tilt angles with respect to the membrane normal. The peak parameters, intensity, width (HWHM) ω, and position q_0, evaluated as functions of ϕ, give information about the

flexibility of the chains, the ratio of tilted chains, and the inter-chain distance of $a = 4.9$ Å. In (b), a set of radial slices (dashed curves) for different angles ϕ is displayed, ranging from $\phi = 5°$ (top curve) to $\phi = 90°$ (bottom curve). The data show a systematic decrease of the peak maximum, accompanied by an increase of its width. This behaviour has been tentatively interpreted as follows: the intensity scattered into the direction of ϕ is attributed to a population of chain segments tilted with respect to the bilayer normal. It is therefore a measure for the angular distribution of the chains. The constant peak position indicates that tilted chains (or chain segments) are characterized by the same mean inter-chain distance. The increasing width $\omega(\phi)$ reflects the decreasing correlation length $\xi(\phi)$ of the tilted segments. With this interpretation, the distribution of tilt angles can be determined by normalization to the integrated intensities. However, the present interpretation in the form of populations of tilted segments must be regarded with caution. A better description is based on the joint refinement of scattering and MD simulation data, which can be Fourier transformed and compared to the measured 2D intensity distribution.

The chain positions in the plane of the bilayer plane are described by a 2D point field (fluid), which is generated by the intersection between the hydrocarbon chains and a plane at constant z in the hydrophobic region. This 2D liquid has a characteristic radial distribution function $g(r)$, which is probed in reciprocal space by a slice through the chain correlation peak at $\phi \simeq 0$. The radial distribution function can also be written as the Fourier Bessel transform of the structure factor:

$$g(r) = \frac{1}{2\pi\rho} \int [S(q) - 1] J_0(qr) q \, \mathrm{d}q, \tag{12}$$

which is experimentally found to exhibit a Lorentzian lineshape,

$$S(q) = I \frac{\omega^2}{(q - q_0)^2 + \omega^2} + y_0, \tag{13}$$

where I denotes the peak intensity, ω the HWHM, q_0 the centre and y_0 the baseline of the peak. Evaluating the integral, it was found that if the width of the peak is small compared to the peak centre, $\omega/q_0 \ll 1$, $g(r)$ can be well approximated by

$$g(r) \simeq 1 + \frac{I\omega}{\rho} \sqrt{\frac{q_0}{2\pi}} \frac{\mathrm{e}^{-r/\xi}}{\sqrt{r}} \cos(q_0 r - \pi/4). \tag{14}$$

Note that this form of $g(r)$ implies that there are no higher q oscillations in $S(q)$ observed. From equation (14) one can determine the correlation length $\xi = \omega^{-1}$ of the exponential decay and, most importantly, the period $\frac{2\pi}{q_0}$ as well as the phase shift $\pi/4$ of the oscillatory term. The resulting chain–chain distance defined as the first maximum of $g(r)$ is calculated approximately as

$$a \simeq \frac{9\pi}{4q_0} - \frac{3\omega}{2q_0^2}. \tag{15}$$

This analysis has been confirmed by comparison with lipid coordinates obtained from molecular dynamics (MD) simulation, carried out on 200 hydrated POPC molecules [22]. The two-dimensional structure factor has been calculated by Fourier transforming the atom coordinates. An additional peak at $q_r = 0.8$ Å^{-1} observed in the MD structure factor was observed experimentally only close to the main phase transition of the lipid, and can be attributed to short range ordering of the head groups. The simulated bilayer was cut into slices at fixed z; the radial distribution functions $g(r)$ and the structure function $S(q)$ showed excellent agreement with the functional forms used above.

Let us now turn to the example of a recent inelastic scattering experiment on the model system DMPC (-d54, deuterated 1,2-dimyristoyl-sn-glycero-3-phoshatidylcholine), where the

structure factor $S(Q_r, \omega)$ was measured in the gel ($P_{\beta'}$) and fluid (L_α) phase. A detailed description of the experimental set-up and method can be found in [108]. Figure 12(c) shows the dispersion relation in the gel and the fluid phase as measured by several constant-q scans at q-values ranging from $q = 0.7$ to $3.0\,\text{Å}^{-1}$. At small lateral momentum transfer q_r, longitudinal sound waves in the plane of the bilayer are probed and give rise to a linear increase of $\omega \propto q_r$, saturating at some maximum value ('maxon'), before a pronounced minimum Ω_0 ('roton') is observed at $q_0 \simeq 1.4\,\text{Å}^{-1}$, the first maximum in the static structure factor $S(q_r)$ (the inter-chain correlation peak). Qualitatively, this can be understood if q_0 is interpreted as the quasi-Brillouin zone of a two-dimensional liquid. Collective modes with a wavelength of the average nearest neighbour distance $2\pi/q_0$ are energetically favourable, producing a minimum. At q_r values well above the minimum, the dispersion relation is dominated by single-particle behaviour. A quantitative theory which predicts the absolute energy values of 'maxon' and 'roton' on the basis of molecular parameters is absent so far. However, the dispersion relation can be extracted from molecular dynamics (MD) simulations by temporally and spatially Fourier transforming the molecular real space coordinates [109] and shows excellent agreement. The INS data are less noisy and cover a wider range as compared to IXS [105].

Temperature-dependent (elastic) q-scans have been performed through the inter-acyl-chain peak in the temperature range from $T = 20$ to $40\,^\circ\text{C}$ to probe the static correlations in the plane of the bilayer as a function of T. As is well known, when going from the gel to the fluid phase, the peak position changes to smaller q_r-values (larger average next neighbour distances) and the peaks broaden, indicating a decreasing correlation length ξ_r in the plane of the membranes. Although the phase transition is of first order [99, 6, 7], the structural values of next neighbour distance a, correlation length ξ, and bilayer thickness point to a critical (anomalous) behaviour of the bilayer. In the inelastic experiments, small traces of the 'fluid excitation' were found already in the gel phase. Conversely, at $T = 30\,^\circ\text{C}$, far into the fluid phase, the 'gel excitation' was still observed, indicating a coexistence of fluid and gel domains. This coexistence was observed in the range of the dispersion minimum which coincides with the maximum of the static structure factor. At the same time, the elastic scans did not show coexistence of two phases, but the typical well known behaviour: while the transition is of first order, a pseudo-critical swelling, i.e. a continuous change of the interlamellar distance in the range of T_c, is observed for DMPC and other lipids [6, 99, 110]. The changes in d are accompanied by corresponding changes in the mean distance between chains. For both quantities, the elastic diffraction data show a continuous change, while the interpretation of the inelastic curves indicates a coexistence of gel and fluid domains, in particular also far above the transition in the fluid phase.

9. Conclusions

The results of the preceding sections show that scattering from aligned membranes may be used as a tool to elucidate bilayer structure and interaction properties on the basis of changing fluctuation and elasticity properties. To this end, an appropriate model is needed. Currently, the linear smectic model is almost exclusively used in the analysis, while a model-independent analysis shows systematic deviations, regardless of whether the comparison is mode in real or reciprocal space. In our eyes, the limits of the linear model become apparent, even though it is still unclear due to which predominant effect. The scattering distribution can only partially be described by linear smectic (Caillé) theory. A generalized theory with corresponding parameters is still lacking and could stimulate the further use of non-specular reflectivity.

We also note that only a few limited methods are currently available to determine the fundamental smectic length scale Λ or the bilayer bending rigidity κ. While light scattering or

optical microscopy techniques determine κ from thermal fluctuations on much larger length scales, which may lead to different values, x-ray powder diffraction and lineshape analysis is sensitive to Λ only in the limit of very soft and strongly undulating systems, untypical for phospholipids. By non-specular neutron and x-ray scattering from aligned phases the bilayer structure and fluctuation is accessible over a wide range both for relatively stiff and soft systems. At the same time, future studies should also concentrate on the temporal (dynamic) behaviour to gain a better understanding of lipid bilayers, both on the molecular and the mesoscopic length scales. To this end, measurements of the collective short wavelength dynamics in lipid bilayers are of importance because the collective dynamics are likely to play a crucial role for different biological functions. The use of a triple-axis spectrometer allows us to measure structure and dynamics, i.e. reflectivity, acyl chain correlation peak and in-plane dynamics. Neutron spin echo and x-ray photon correlation spectroscopy may be used in future to probe the collective dynamics on mesoscopic length scales.

Acknowledgments

We are indebted to D Constantin, W Fenzl, C Li, U Mennicke, C Münster, L Perino-Gallice, A Spaar, and M Vogel for the enjoyable and fruitful collaborations with regard to different original studies described here, as well as our colleges at the synchrotron radiation and neutron sources HASYLAB, ESRF, and ILL, where data was taken. Michael Vogel has been the key person in the studies of thermal unbinding (figures 10 and 11), and has made significant contributions in measuring and analysing the diffuse scattering of aligned phases in his PhD. The oligo-membrane work (figures 6 and 7) was predominantly pursued in the PhD work of Ulrike Mennicke, who has achieved full q_z range fits, and has studied the interaction forces as a function of osmotic pressure. Chenghao Li is acknowledged for his contributions to x-ray reflectivity, both measurement and analysis, and Alexander Spaar for his leading role in the investigation of acyl chain packing and analysis of the chain correlation peak (figure 12(a)). Finally, I would like to emphasize the contributions of Maikel Rheinstaedter as the key scientist in recent and ongoing studies of membrane dynamics by inelastic neutron scattering (figure 12(b)).

Financial aid by the Deutsche Forschungsgemeinschaft (DFG) through grants SA 772/3 and SA-772/4 and by the German Research Ministry under contract number 05KS1TSA7 is gratefully acknowledged.

References

[1] Lipowsky R and Sackmann E (ed) 1995 *Structure and Dynamics of Membranes* (*Handbook of Biological Physics* vol 1) (Amsterdam: Elsevier, North-Holland)
[2] Koltover I, Salditt T, Rädler J O and Safinya C R 1998 *Science* **281** 78
[3] Koltover I, Rädler J O, Salditt T and Safinya C R 1999 *Phys. Rev. Lett.* **82** 3184
[4] Safinya C R, Sirota E B, Roux D and Smith G S 1986 *Phys. Rev. Lett.* **57** 2718
[5] Safinya C R, Sirota E B, Roux D and Smith G S 1989 *Phys. Rev. Lett.* **62** 1134
[6] Nagle J F, Petrache H I, Gouliaev N, Tristram-Nagle S, Liu Y, Suter R M and Gawrisch K 1998 *Phys. Rev.* E **58** 7769
[7] Petrache H I *et al* 1998 *Phys. Rev.* E **57** 7014
[8] de Jeu W, Ostrovskii B I and Shalaginov A 2003 *Rev. Mod. Phys.* **75** 181
[9] Rand R P and Parsegian V A 1989 *Biochim. Biophys. Acta* **988** 351
[10] Israelachvili J N 1985 Intermolecular and surface forces (New York: Academic)
[11] Smith G S, Sirota E B, Safinya C R, Plano R J and Clark N A 1990 *J. Chem. Phys.* **92** 4519
[12] Katsaras J 1995 X-ray diffraction studies of oriented lipid bilayers *Biochem. Cell. Biol.* **73** 209
[13] Katsaras J and Raghunathan V A 2000 Lipid bilayers; structure and interactions ed J Katsaras and T Gutberlet (Berlin: Springer)
[14] Salditt T, Münster C, Lu J, Vogel M, Fenzl W and Souvorov A 1999 *Phys. Rev.* E **60** 7285

[15] Lyatskaya Y, Liu Y, Tristram-Nagle S, Katsaras J and Nagle J F 2001 Method for obtaining structure and interactions from oriented lipid bilayers *Phys. Rev.* E **63** 011907–011915
[16] Bayerl T M, Thomas R K, Rennie A, Penfold J and Sackmann E 1991 *Biophys. J.* **60** 1
[17] Fragneto G, Charitat T, Graner F, Mecke K, Perino-Gallice L and Bellet-Amalrice E 2001 A fluid floating bilayer *Europhys. Lett.* **53** 100
[18] Kuhl T L, Majewski J, Wong J Y, Steinberg S, Leckband D E, Israelachvili J N and Smith G S 1998 *Biophys. J.* **75** 2352
[19] Lösche M 2002 Surface-sensitive x-ray and neutron scattering characterization of planar lipid model membranes and lipid/peptide interactions *Curr. Top. Membranes* **52** 117
[20] Tolan M 1999 *X-ray Scattering from Soft-Matter Thin Films* (*Springer Tracts in Modern Physics* vol 148) (Berlin: Springer)
[21] Als-Nielsen J and McMorrow D 2001 *Elements of Modern X-Ray Physics* (New York: Wiley)
[22] Heller H, Schaefer M and Schulten K 1993 *J. Phys. Chem.* **97** 8343
[23] Seul M and Sammon M J 1990 *Thin Solid Films* **185** 287
[24] Smith G, Sirota E B, Safinya C R and Clark N A 1988 Structure of the L_β phases in a hydrated phosphatidylcholine multimembrane *Phys. Rev. Lett.* **60** 813
[25] Mennicke U and Salditt T 2002 *Langmuir* **18** 8172
[26] Münster C M, Salditt T, Vogel M, Siebrecht R and Peisl J 1999 *Europhys. Lett.* **46** 486
[27] Perino-Gallice L, Fragneto G, Mennicke U, Salditt T and Rieutord F 2002 Dewetting of solid-supported multilamellar lipid layers *Eur. Phys. J.* E **8** 275
[28] Nagle J F and Katsaras J 1999 *Phys. Rev.* E **59** 7018
[29] Vogel M, Münster C, Fenzl W and Salditt T 2000 *Phys. Rev. Lett.* **84** 390
[30] Parsegian V A, Rand R P, Fuller N L and Rau D C 1986 Osmotic stress for the direct measurement of intermolecular forces *Methods in Enzymology* vol 127, ed L Packer (New York: Academic)
[31] Dubois M and Zemb Th 1998 Elastic properties of lipid bilayer: Theory and possible experiments *J. Physique Coll.* **8** 55–62
[32] Katsaras J 1997 Highly aligned lipid membrane systems in the physiologically relevant 'excess water' condition *Biophys. J.* **73** 2924
[33] Brotons G, Salditt T, Dubois M and Zemb Th 2003 Highly oriented, charged multilamellar membranes osmotically stressed by a polyelectrolyte of the same sign *Langmuir* **19** 8235
[34] Helfrich W 1973 *Z. Naturf.* c **28** 693
[35] Münster C 2000 *PhD Dissertation* Universität München
[36] Schreyer A, siebrecht R, Englisch U, Pietsch U and Zabel H 1998 *Physica* B **248** 349
[37] Cubitt R and Fragneto G 2003 *Appl. Phys.* A **74** 329
[38] Salditt T, Münster C, Mennicke U, Ollinger C and Fragneto G 2003 *Langmuir* **19** 7703
[39] Rheinstädter M, Ollinger C, Fragneto-Cusani G and Salditt T 2004 Collective dynamics of lipid membranes studied by inelastic neutron scattering *Phys. Rev. Lett.* **93** 108107
[40] Lei N, Safinya C R and Bruinsma R 1995 *J. Physique* II **5** 1155
[41] Lei N 1993 *PhD Thesis* Rutgers
[42] Caillé A 1971 *C. R. Acad. Sci.* **274** 891
[43] Holyst R, Tweet D J and Sorensen L B 1990 *Phys. Rev. Lett.* **65** 2153
[44] Constantin D, Mennicke U, Li C and Salditt T 2003 *Eur. Phys. J.* E **12** 283–90
[45] Als-Nielsen J, Litster J D, Birgenau R J, Kaplan M and Safinya C R 1980 *Phys. Rev.* B **22** 312
[46] Sinha S K, Sirota E B, Garoff S and Stanley H B 1988 *Phys. Rev.* B **38** 2297
[47] Sinha S K 1994 *J. Physique* III 4
[48] Salditt T, Vogel M and Fenzl W 2003 *Phys. Rev. Lett.* **90** 178101
[49] Ollinger C, Constantin D, Seeger J and Salditt T 2004 Lipid membranes on silicon surface grating studied by neutron reflectivity *Eur. Phys. Lett.* submitted
[50] Sens P and Turner M S 1997 *J. Physique* II **7** 1855
[51] Sens P and Turner M S 1997 Inclusions in thin smectic films *J. Physique* II **7** 1855–1870
[52] Turner M S and Sens P 1997 Interactions between particulate inclusions in a smectic—a liquid crystal *Phys. Rev.* E **55** 1275–78
[53] Turner M S and Sens P 1998 Multipole expansion for inclusions in a lamellar phase *Phys. Rev.* E **57** 823–8
[54] Gouliaev N and Nagle J F 1998 Simulations of interaction membranes in the soft confinement regime *Phys. Rev. Lett.* 2610–93
[55] Mecke K R, Charitat T and Graner F 2003 *Langmuir* **19** 2080–7
[56] Netz R R and Lipowsky R 1993 *Phys. Rev. Lett.* **71** 3596–9
[57] Gao L and Golubovic L 2003 *Phys. Rev.* E **67** 021708

[58] Mennicke U, Constantin D and Salditt T 2004 Structure and interaction potentials in solid-supported lipid membranes studied by x-ray reflectivity at varied osmotic pressure *Phys. Rev.* E submitted
[59] Gompper G and Kroll D M 1998 Membranes with fluctuation topology: Monte Carlo simulations *Phys. Rev. Lett.* **81** 2284–7
[60] Goetz R, Gompper G and Lipowsky R 1998 Mobility and elasticity of self-assembled membranes *Phys. Rev. Lett.* **82** 221–847
[61] Boeckmann R 2003 *PhD Thesis* Göttingen University
[62] Rand R P 1981 *Annu. Rev. Biophys. Bioeng.* **10** 227
[63] Leikin S, Rau D C, Parsegian V A and Rand R P 1993 *Annu. Rev. Phys. Chem.* **44** 369
[64] Marcelja S and Radic N 1976 *Chem. Phys. Lett.* **49** 129
[65] Kornyshev A A and Leikin S 1989 *Phys. Rev.* A **40** 6431
[66] Leikin S and Kornyshev A A 1990 *J. Chem. Phys.* **92** 6890
[67] Israelachvili J and Wennerstoem H 1996 *Nature* **379** 219
[68] Parsegian A P 2005 *van der Waals Forces* (Cambridge: Cambridge University Press)
[69] Derjaugin B V, Churjaev N V and Müller V M 1987 *Surface Forces* (New York: Consultants Bureau)
[70] Parsegian V A and Ninham B W 1973 *J. Theor. Biol.* **38** 101
[71] Fenzl W 1995 *Z. Phys.* B **97** 333–6
[72] Petrache H I, Gouliaev N, Tristram-Nagle S, Zhang R, Suter R M and Nagle J F 1998 *Phys. Rev.* E **57** 7014–24
[73] Mennicke U 2003 Structure and fluctuations of solid-supported phospholipid membranes *PhD Thesis* Göttingen University (in German)
[74] Lipowsky R 1995 Generic interactions of flexible membranes *Handbook of Biological Physics* vol 1, ed R Lipowsky and E Sackmann (Amsterdam: Elsevier Science) pp 521–602
[75] Pynn R 1992 *Phys. Rev.* B **45** 602
[76] Salditt T, Li C, Spaar A and Mennicke U 2002 X-ray reflectivity of solid-supported multilamellar membranes *Eur. Phys. J.* E **7** 105
[77] Pabst G, Rappolt M, Amenitsch H and Laggner P 2000 Structural information from multilamellar liposomes at full hydration: full q-range fitting with high quality x-ray data *Phys. Rev.* E **62** 4000
[78] Blaurock A E 1982 Evidence of bilayer structure and of membrane *Biochem. Biophys. Acta* **650** 167
[79] Li C, Constantin D and Salditt T 2004 Biomimetic membranes of lipid–peptide model systems prepared on solid support *J. Phys.: Condens. Matter* **16** S2439–53
[80] Salditt T 2000 *Curr. Opin. Colloid Interface Sci.* **19** 232
[81] Fragneto G, Charitat T, Bellet-Amalric E, Cubitt R and Graner F 2003 Swelling of phospholipid floating bilayers: the effect of chain length *Langmuir* **19** 7695–702
[82] Vogel M, Münster C, Fenzl W, Thiaudière D and Salditt T 2000 Fully hydrated and highly oriented membranes: an experimental setup amenable to specular and diffuse x-ray scattering *Physica* B **283** 32
[83] Caille A 1972 *C. R. Acad. Sci. Paris* B **274** 891
[84] Salditt T, Vogel M and Fenzl W 2003 *Phys. Rev. Lett.* **90** 178101 (erratum)
[85] Chu N, Kucerka N, Liu Y, Tristram-Nagle S and Nagle J F, Anomalous swelling of lipid bilayer stacks is caused by softening of the bending modulus *Preprint*
[86] Pabst G, Katsaras J and Raghunathan V A 2002 Enhancement of steric repulsion with temperature in oriented lipid multilayers *Phys. Rev. Lett.* **88** 128101
[87] Petrache H, Tristam-Nagle S and Nagle J F 1998 *Chem. Phys. Lipids* **95** 83
[88] Rawicz W, Olbrich K C, McIntosh T, Needham D and Evans E 2000 *Biophys. J.* **79** 328–39
[89] Pabst G, Katsaras J, Raghunathan V A and Rappolt M 2003 *Langmuir* **19** 1716–22
[90] Liu Y and Nagle J F, Diffuse scattering provides material parameters and electron density profiles of biomembranes *Phys. Rev.* E **69** 04091(R)
[91] Vogel M 2000 Röntgenbeugung an hochorientierten phospholipidmembranen *PhD Dissertation* Universität Potsdam
[92] Vogel M, Münster C, Fenzl W and Salditt T 2000 *Phys. Rev. Lett.* **84** 390–3
[93] Netz R R and Lipowsky R 1993 *Phys. Rev. Lett.* **71** 3596
[94] Ollinger C 2003 Structure and interactions of solid-supported bilayers in external electric fields *Diploma Thesis* University of Saarland (in German)
[95] Constantin D, Ollinger C and Salditt T
[96] Pozo-Navas B, Raghunathan V A, Katsaras J, Rappolt M, Lohner K and Pabst G 2003 *Phys. Rev. Lett.* **91** 028101
[97] Lemmich J, Mortensen K, Ipsen J H, Honger T, Bauer R and Mouritsen O G 1995 Pseudocritical behaviour and unbinding of phospholipid bilayers *Phys. Rev. Lett.* **75** 3958

[98] Zhang R, Sun W, Tristram-Nagle S, Headrick R L, Suter R M and Nagle J F 1996 Critical fluctuations in membranes *Phys. Rev. Lett.* **74** 2132
[99] Chen F Y, Hung W C and Huang H W 1997 *Phys. Rev. Lett.* **79** 4026
[100] Harroun T A, Nieh M-P, Watson J, Raghunathan V A, Pabst G, Morrow M R and Katsaras J 2004 *Phys. Rev.* E **69** 031906
[101] Bayerl T 2000 *Curr. Opin. Colloid Interface Sci.* **5** 232
[102] Paula S, Volkov A G, Van Hoek A N, Haines T H and Deamer D W 1996 *Biophys. J.* **70** 339
[103] Pfeiffer W, Henkel Th, Sackmann E and Knorr W 1989 *Europhys. Lett.* **8** 201
[104] Nevzorov A A and Brown M F 1997 *J. Chem. Phys.* **107** 10288
[105] Chen S H, Liao C Y, Huang H W, Weiss T M, Bellisent-Funel M C and Sette F 2001 *Phys. Rev. Lett.* **86** 740
[106] Spaar A and Salditt T 2003 *Biophys. J.* **85** 1
[107] Rheinstädter M C, Ollinger C, Fragneto G and Salditt T 2004 Collective dynamics of lipid membranes studied by inelastic neutron scattering *Phys. Rev. Lett.* **93** 108107-1–108107-4
[108] Rheinstädter M C, Ollinger C, Fragneto G and Salditt T *Physica* B **350** 136
[109] Tarek M, Tobias D J, Chen S-H and Klein M L 2001 *Phys. Rev. Lett.* **87** 238101
[110] Mason P C, Nagle J F, Epand R M and Katsaras J 2001 *Phys. Rev.* E **63** 030902(R)